Research Paper

THEMED ISSUE: Origin and Evolution of the Sierra Nevada and Walker Lane

GEOSPHERE

GEOSPHERE; v. 11; no. 3

doi:10.1130/GES00821.1

13 figures; 1 table

CORRESPONDENCE: kell@seismo.unr.edu

CITATION: Eisses, A.K., Kell, A., Kent, G.M., Driscoll, N.W., Baskin, R.L., Smith, K.D., Karlin, R.E., Louie, J.N., and Pullammanappallil, S.K., 2015, New constraints on fault architecture, slip rates, and strain partitioning beneath Pyramid Lake, Nevada: Geosphere, v. 11, no. 3, p. 683–704, doi:10.1130/GES00821.1.

Received 16 May 2012
Revision received 21 January 2015
Accepted 26 March 2015
Published online 13 May 2015

New constraints on fault architecture, slip rates, and strain partitioning beneath Pyramid Lake, Nevada

Amy Kendra Eisses[1], Annie Kell[1], Graham Martin Kent[1], Neal William Driscoll[2], Robert LeRoy Baskin[3], Ken Dent Smith[1], Robert Ellis Karlin[4], John Nikolai Louie[1], and Satish Kumar Pullammanappallil[5]

[1]Nevada Seismological Laboratory, University of Nevada, Reno, 1664 North Virginia Street, MS0174, Reno, Nevada 89557-0174, USA
[2]Scripps Institution of Oceanography, University of California, San Diego, 9500 Gilman Drive #0244, La Jolla, California 92093-0244, USA
[3]U.S. Geological Survey, 2222 West 2300 South, 2nd floor, Salt Lake City, Utah 84119 USA
[4]Department of Geological Sciences and Engineering, University of Nevada, Reno, Geological Sciences and Engineering (0172), 1664 North Virginia Street, Reno, Nevada 89557, USA
[5]Optim, Inc., 200 South Virginia Street, Suite 560, Reno, Nevada 89501, USA

ABSTRACT

A seismic compressed high-intensity radar pulse (CHIRP) survey of Pyramid Lake, Nevada, defines fault architecture and distribution within a key sector of the northern Walker Lane belt. More than 500 line-kilometers of high-resolution (decimeter) subsurface imagery, together with dated piston and gravity cores, were used to produce the first comprehensive fault map and attendant slip rates beneath the lake. A reversal of fault polarity is observed beneath Pyramid Lake, where down-to-the-east slip on the dextral Pyramid Lake fault to the south switches to down-to-the-west displacement on the Lake Range fault to the north. Extensional deformation within the northern two thirds of the basin is bounded by the Lake Range fault, which exhibits varying degrees of asymmetric tilting and stratal divergence due to along-strike segmentation. This structural configuration likely results from a combination of changes in slip rate along strike and the splaying of fault segments onshore. The potential splaying of fault segments onshore tends to shift the focus of extension away from the lake. The combination of normal- and oblique-slip faults in the northern basin gives Pyramid Lake its distinctive "fanning open to the north" geometry. The oblique-slip faults in the northwestern region of the lake are short and discontinuous in nature, possibly representing a nascent shear zone. In contrast, the Lake Range fault is long and well defined. Vertical slip rates measured across the Lake Range and other faults provide new estimates on extension across the Pyramid Lake basin. A minimum vertical slip rate of ~1.0 mm/yr is estimated along the Lake Range fault. When combined with fault length, slip rates yield a potential earthquake magnitude range between M6.4 and M7.0. Little to no offset on the Lake Range fault is observed in the sediment rapidly emplaced at the end of Tioga glaciation (12.5–9.5 ka). In contrast, since 9.5 ka, CHIRP imagery provides evidence for three or four major earthquakes, assuming a characteristic offset of 2.5 m per event. Regionally, our CHIRP investigation helps to reveal how strain is partitioned along the boundary between the northeastern edge of the Walker Lane and the northwest Basin and Range Province proper.

INTRODUCTION AND RATIONALE

Dextral shear is unevenly distributed along the western margin of North America, with ~75%–80% of the Pacific and North American plate motion being accommodated by the San Andreas fault and other fault systems to the west (Bennett et al., 1999; Dixon et al., 2000). The remaining deformation occurs east toward the Basin and Range Province (e.g., Atwater, 1970; Atwater and Stock, 1998; McQuarrie and Wernicke, 2005). The structurally complex transition between the Sierra Nevada microplate and the Basin and Range (Fig. 1), known as the Walker Lane deformation belt to the north and the Eastern California shear zone to the south, is identified by seismic, geodetic, and geologic data (e.g., Locke et al., 1940; Stewart, 1988; Dokka and Travis, 1990; Argus and Gordon, 1991; Thatcher et al., 1999; Svarc et al., 2002; Bennett et al., 2003; Unruh et al., 2003; Oldow, 2003; Hammond and Thatcher, 2004; Wesnousky, 2005a, 2005b; Wesnousky et al., 2005). This ~100-km-wide belt of seismicity and active faulting accommodates up to 20%–25% or 8–13 mm/yr of relative motion between the Sierra Nevada microplate and stable North America plate (Thatcher et al., 1999; Thatcher, 2003; Bennett et al., 2003; Hammond et al., 2011). Studies show that most of the deformation in the Walker Lane belt occurs along the eastern and western margins of the belt (Hammond et al., 2011). Furthermore, seismicity is concentrated at the eastern and western boundaries of the Basin and Range, with higher rates of strain localized on the western side within the Central Nevada seismic belt and the Walker Lane (Eddington et al., 1987).

Pyramid Lake is located toward the eastern margin of the northern Walker Lane belt in a transitional zone between two distinct geological regions: the Walker Lane deformation belt and the Basin and Range Province (Fig. 1). Within the Pyramid Lake region, transtension is accommodated through a series of mainly dextral oblique strike-slip faults (Turner et al., 2008). Northwest of Pyramid Lake (e.g., Honey Lake fault zone; Fig.1), dextral faults strike northwest, whereas toward the southwest, north-striking, normal fault–bounded basins predominate (e.g., Lake Tahoe Basin; Dingler et al., 2009). South of Pyramid Lake, within the Carson domain (Stewart,

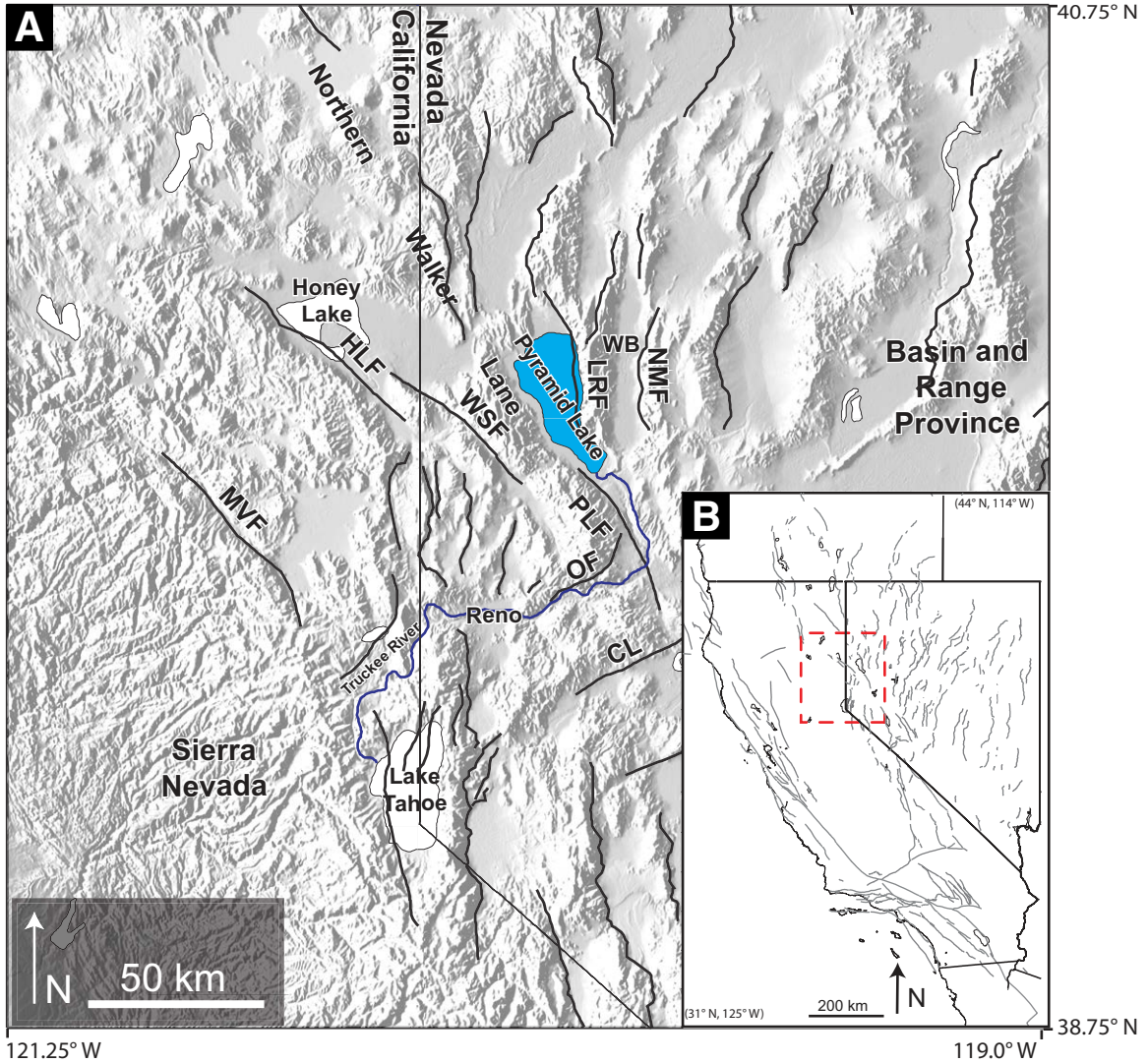

Figure 1. (A) Map of the northern Walker Lane deformation belt, northwest Basin and Range Province, and northern Sierra Nevada microplate. River and state boundary lines are dark gray, and faults are thin black lines. Pyramid Lake is shaded in light blue, and the Truckee River is dark blue. CL—Carson Lineament; HLF—Honey Lake fault; LRF—Lake Range fault; MVF—Mohawk Valley fault; NMF—Nightingale Mountains fault; OF—Olinghouse fault; PLF—Pyramid Lake fault; WB—Winnemucca Basin; WSF—Warm Springs Valley fault. (B) Regional map of the western United States; red box shows the enlarged map of the northern Walker Lane deformation belt shown in A.

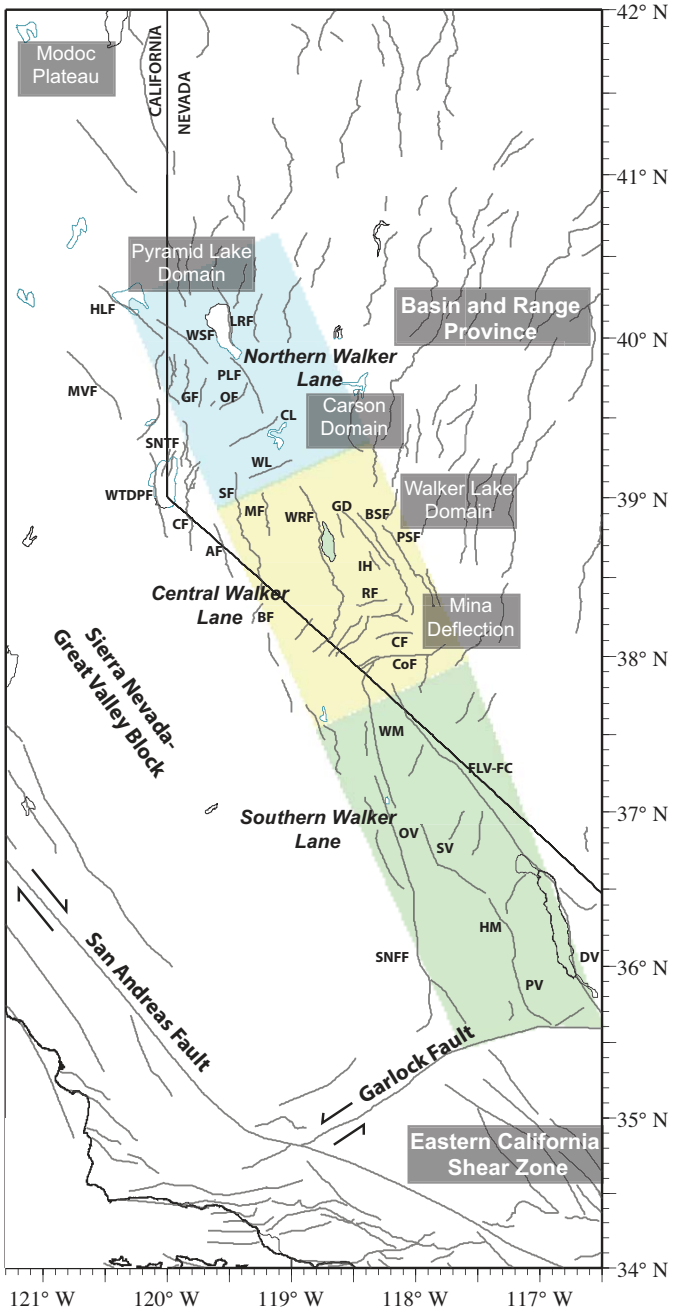

1988), a more complex pattern of deformation is observed (Fig. 2), characterized by significant amounts (>30°) of clockwise vertical-axis rotation bounded by ENE-striking sinistral faults (Cashman and Fontaine, 2000).

Pyramid Lake is a remnant of Pleistocene lakes that once covered much of the Great Basin during the late Pleistocene. The two largest of these lakes were Lake Bonneville and Lake Lahontan (Gilbert, 1890; Adams et al., 1999). At its highstand, Lake Lahontan straddled the boundary between the Walker Lane region and the central Basin and Range Province (Adams et al., 1999). The deepest point of ancient Lake Lahontan is within the present-day Pyramid Lake basin (Benson and Mifflin, 1986).

The stratigraphy of Pyramid Lake provides a detailed record of the geologic and tectonic history of the basin. The low wave energy of the hydrologic system preserves the stratigraphy and chronicles the tectonic deformation (e.g., Kent et al., 2005; Dong et al., 2014). The asymmetric (i.e., half-graben) geometry creates differential accommodation, which records and preserves the deformation. Remnant sections of ancient Lake Lahontan (i.e., Pyramid Lake) provide ideal opportunities to investigate the rapidly deforming northern Walker Lane belt (Adams et al., 1999; Thatcher et al., 1999). Many remnant sections of Lake Lahontan have been targets for extensive paleoclimate studies, including cores used for chronostratigraphic analysis. Cores collected from Pyramid Lake highlight a nearly continuous record of sedimentation extending to 48 ka (Benson et al., 2013).

The Pyramid Lake basin provides an ideal natural laboratory in which to study transtensional deformation in the northern Walker Lane. In June 2010, the University of Nevada, Reno, Scripps Institution of Oceanography, and the U.S. Geological Survey acquired more than 500 line-kilometers of decimeter-resolution seismic imagery in Pyramid Lake, Nevada. The compressed high-intensity radar pulse (CHIRP) seismic system images beneath the lake to ~70 m depth, allowing fault mapping and measurement of stratigraphic offsets. These features record the structural evolution of the complex Pyramid Lake basin. Five dated sediment cores from previous paleoclimate investigations (Mensing et al., 2004; Benson et al., 2002, 2013), together with the CHIRP profiles, provide a chronostratigraphic framework for the lake.

Fault locations were refined in the marine setting and then correlated to mapped faults on land. The stratigraphic offset and sense of dip across faults observed on CHIRP records were documented and compared to displacements

Figure 2. Map of the Walker Lane deformation belt showing the locations of the northern, central, and southern Walker Lane and their respected regions with associated major faults. AF—Antelope fault; BF—Bridgeport fault; BSF—Benton Spring fault; CF—Carson fault; CL—Carson Lineament; CoF—Coaldale fault; DV—Death Valley fault; FLV-FC—Fish Lake Valley–Furnace Creek fault; GD—Gumdrop Hills fault; GF—Genoa fault; HLF—Honey Lake fault; HM—Hunter Mountain fault; IH—Indian Head fault; LRF—Lake Range fault; MF—Mason fault; MVF—Mohawk Valley fault; OF—Olinghouse fault; OV—Owens Valley fault; PLF—Pyramid Lake fault; PSF—Petrified Spring fault; PV—Panamint Valley; RF—Rattlesnake fault; SF—Smith fault; SNFF—Sierra Nevada frontal fault; SNTF—Stateline–North Tahoe fault; SV—Saline Valley fault; WL—Wabuska Lineament; WM—White Mountain fault; WRF—Wassuk range-front fault; WSF—Warm Springs Valley fault; WTDPF—West Tahoe–Dollar Point fault.

observed on adjacent profiles in order to correlate fault trace locations. The resulting fault map not only contributes to understanding of strain partitioning in this basin, but also in classifying earthquake hazards for nearby metropolitan areas around the lake (e.g., Reno and Sparks, Nevada). Furthermore, a suite of piston and gravity cores (Benson et al., 2013) provided down-core age estimates to assist in calculating rates across offset sediments, placing important constraints on slip rates and earthquake history.

WALKER LANE GEOLOGIC SETTING

The Walker Lane deformation belt and Eastern California shear zone are regions of northwest-striking, right-lateral shear that separate the Sierran microplate (Sierra Nevada–Great Valley block) from the larger Basin and Range Province (Stewart, 1988; Faulds and Henry, 2008; Fig 2). The Walker Lane is subdivided into northern, central, and southern provinces (colored regions in Fig. 2). The southern Walker Lane extends from the Garlock fault northward to the Mina deflection and consists of dominantly northwest-striking, broadly overlapping dextral faults. The central Walker Lane consists of the Coaldale domain and the Walker Lake domain. The Mina deflection is a complex series of northwest-striking dextral faults, northeast-striking normal faults, and east- to east-northeast–striking sinistral faults (Stewart, 1988; Oldow, 1992; Wesnousky, 2005a; Faulds and Henry, 2008; Nagorsen-Rinke et al., 2013). To the north, the Walker Lake domain is a region of dextral shear containing northwest- to north-northwest–striking left-stepping dextral faults (Stewart, 1988; Ekren et al., 1980; Hardyman, 1980; Ekren and Byers, 1984). Finally, the northern Walker Lane is made up of the Carson domain, Pyramid Lake domain, and Modoc Plateau domain. The Carson domain is a region of east- to northeast-striking sinistral fault zones and clockwise-rotated fault blocks (Cashman and Fontaine, 2000; Faulds et al., 2005a, 2005b). Farther north, the Pyramid Lake domain is a discrete belt of left-stepping en echelon dextral faults (Briggs and Wesnousky, 2004; Briggs and Wesnousky, 2005a; Drakos, 2007). The Modoc Plateau domain is a zone of widely spaced northwest-striking faults and lineaments that extend to the southern Cascade arc (Faulds and Henry, 2008; Trexler et al., 2009).

The tectonic development of the Eastern California shear zone and the Walker Lane is closely linked with the evolution of the San Andreas fault system (Fig. 2), which initiated ca. 30 Ma (Atwater, 1970). The northern Walker Lane (i.e., Pyramid Lake domain) is the youngest and thus least-developed segment of the Walker Lane. The cumulative right-lateral displacement decreases from >60 km in southern and central California, to ~25 km in northwest Nevada, to essentially no dextral slip in northeast California (Faulds and Henry, 2008). Faulds et al. (2005a) reported a cumulative right-lateral offset of greater than 50 km for faults in the southern Walker Lane, between 34 and 44 km in the central Walker Lane, and ~20–30 km of total slip in the northern Walker Lane. Global positioning system (GPS) geodetic data confirm geological observations that the rate of shear strain across the southern Walker Lane is greater than that of the northern Walker Lane. At ~39°N–40°N latitude, GPS-derived geodetic data show 6 ± 2 mm/yr of northwest-trending dextral shear (Hammond et al., 2011), which accounts for ~15% of Pacific–North America relative motion (Thatcher et al., 1999; Dixon et al., 2000; Thatcher, 2003).

Pyramid Lake Geological Setting

There are two major fault zones in the Pyramid Lake region: the right-lateral Pyramid Lake fault and a west-dipping range-front normal fault along the west side of the Lake Range (Fig. 3). In addition there are series of northwest-trending faults that are located in the northwest quadrant of the lake and come onshore near the Needles formation. In concert with the other basin-bounding faults within the Walker Lane and Great Basin (e.g., Lake Tahoe Basin; Dingler et al., 2009), these faults provide the "fanning to the north" physiography that characterizes the region.

The Pyramid Lake fault zone is one of the major dextral faults in the northern Walker Lane and is located along the eastern boundary of the Walker Lane belt. It is uncertain whether the northwest terminus of this fault lies just south of the lake or if it coincides with the western shoreline (along its southern panhandle portion as shown in Fig. 3). An offset Oligocene paleovalley that is bracketed by Pliocene to late Miocene sediments along the northwestern part of the fault near Pyramid Lake indicates right-lateral deformation of ~5–10 km since the pre–late Miocene to Pliocene (Faulds et al., 2005b). The Pyramid Lake fault has ruptured in four major earthquakes in the Holocene, with inferred right-lateral slip rates of 2.6 ± 0.3 mm/yr (Briggs and Wesnousky, 2004). Chronostratigraphic mapping of Lake Lahontan deposits in the southern part of the basin (Dohrenwend et al., 1991; Bell et al., 2003, 2004) implies that most of the late Quaternary deformation along the Pyramid Lake fault zone has been predominately extensional; the observed vertical offset measurements of 10–26 m in 12–30 ka deposits indicate vertical slip rates as great as ~0.87 mm/yr (Bell and House, 2005).

Farther north, the major basin-bounding fault of the Pyramid Lake basin is the west-dipping Lake Range normal fault. Deep sedimentary basins are observed west of the Lake Range along the eastern margin of the lake (Fig. 3). Drakos (2007) referred to it as the Lake Range fault zone to avoid confusion with the right-lateral Pyramid Lake fault; we adopt this nomenclature. The Lake Range fault has an average strike of N4°W along the eastern shoreline of Pyramid Lake (Fig. 3). In most cases, the surface trace of the fault is located beneath the lake and is observed along the base of the southern Lake Range (Fig. 3). Several large tufa mounds projecting offshore along the eastern edge of the lake provide evidence that the fault trace is submerged just offshore (Drakos, 2007). Since the stratigraphic units on Anaho Island are tilted eastward, Faulds et al. (2003) interpreted that the island is on the hanging wall and is downdropped relative to the Lake Range fault. Such geometry requires a fault strand in the narrow strait east of Anaho Island (Fig. 3; Drakos, 2007). High-resolution digital bathymetry reveals that the greatest relief in Pyramid Lake is along the eastern edge of the lake and the western edge

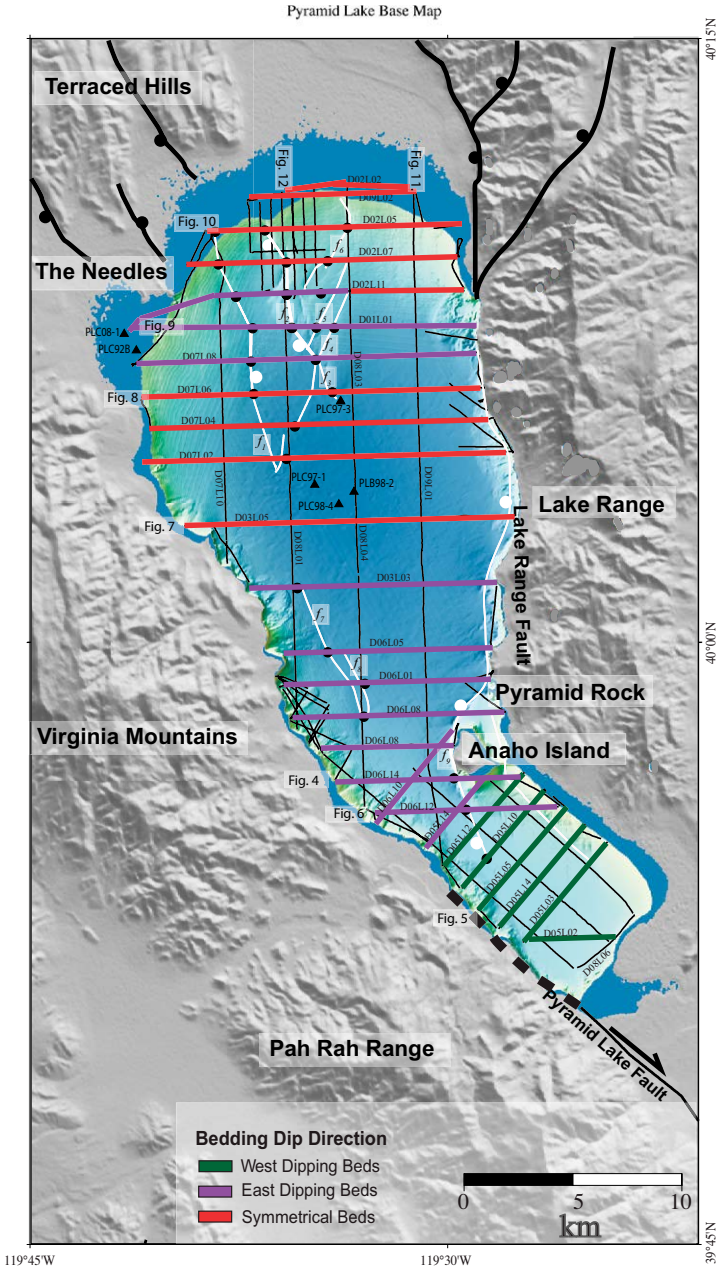

Figure 3. Map of Pyramid Lake, Nevada. The green, purple, red, and light-gray lines within the lake are the compressed high-intensity radar pulse (CHIRP) survey lines. Green lines indicate regional west-dipping reflectors, purple lines designate east-dipping reflectors, red portrays symmetrical, flat-lying horizons, and light-gray lines are the remaining CHIRP survey lines. The white lines are significant faults based on the CHIRP data. The black triangles show the locations of sediment cores collected by Mensing et al. (2004), Benson et al. (2002), and Benson et al. (2013). The black circles are locations where slip rates were calculated within the lake.

of Pyramid Rock, where a steep, ~80-m-high, down-to-the-west escarpment exists (Fig. 3; Drakos, 2007). This continues southward along the western shore of Anaho Island and dies away ~2 km south of the island, marking the observed terminus of the Lake Range fault. Multiple low-sun-angle illuminations of the three-dimensional (3-D) digital elevation model reveal numerous small north- to northeast-striking fault scarps, which appear to be structures linking the southern end of the Lake Range fault and the Pyramid Lake fault farther south of Pyramid Lake (Drakos, 2007).

Slip rates on the Lake Range fault are poorly constrained due to the fact that the majority of the fault is located underwater. The ages of faulted surficial deposits range from late Quaternary to the latest Quaternary (Bonham and Papke, 1969; Dohrenwend et al., 1991; Sawyer and Adams, 1999). A vertical slip rate of 0.6–1.1 mm/yr was estimated by averaging long-term seismic cycles with facet heights (dePolo, 1998); however, the late Quaternary geomorphology along the length of this fault (on-land section) suggests significantly lower recent slip rates of less than 0.2 mm/yr (Sawyer and Adams, 1999).

METHODS

The seismic CHIRP SUBSCAN profiler designed by Scripps Institution of Oceanography and EdgeTech was used to conduct this study. The CHIRP uses swept frequencies ranging from 500 Hz to 15 kHz. The majority of CHIRP profiles collected on Pyramid Lake used a 0.7–3.0 kHz pulse with 50 ms duration. The data were processed using the following steps: (1) Raw data were converted from JSF (CHIRP recording format) to SEGY (standard seismic data format), (2) the analytic (envelope) traces were spatially averaged (5 pings), and (3) averaged traces were converted to depth assuming a nominal 1500 m/s water velocity (e.g., Dingler et al., 2009). A combination of QPS Fledermaus and IHS Kingdom Suite software was used to track horizons, pick faults, and assess the 3-D characteristics of the network of CHIRP profiles.

The data were loaded into the software program IHS Kingdom Suite (http://www.ihs.com/products/oil-gas/geoscience-software/kingdom-seismic-interpretation/index.aspx) for stratigraphic interpretations. Kingdom Suite allows horizon picking and gives the ability to collapse (flatten) layers on either side of a fault. Layer collapsing allows for precise measurement of strata offsets, which record event chronology (such as number and size of earthquake events) and help to constrain the relative time scale of seismic slip. Fledermaus software (http://www.qps.nl/display/fledermaus) requires lines to be converted to

TIFF images, which are georeferenced to ping locations. Using Fledermaus, it was possible to import all the lines into a common scene that assimilated seismic imagery with the topography and bathymetry of the lake basin, giving a clear image of the various data types and the way in which each attribute interrelated in three dimensions. The three-dimensional perspective provided by Fledermaus was most useful in tracking stratigraphic horizons between seismic profiles that crossed a variety of faults.

RESULTS

Over 500 line-kilometers of CHIRP data were acquired in Pyramid Lake (Fig. 3). The survey lines were directed orthogonally, with east-west– and north-south–directed lines in the northern end of the lake. Northeast-southwest and southeast-northwest lines were collected in the "panhandle" southernmost end of the lake. A smaller, dense grid of CHIRP profiles was acquired in the northern end of the basin to confirm the strike of the discontinuous fault systems. The profiles revealed a well-preserved stratigraphic record extending to nearly 50+ m in depth. Imagery revealed fault networks with clear stratigraphic offsets, including growth faulting. Dated stratigraphy from cores established a chronostratigraphy for the region and provided a more complete geological history of faulting and seismic activity in the basin. This section presents the results for our multifaceted investigation, including CHIRP imagery, bathymetry, and sediment cores (Mensing et al., 2004; Benson et al., 2002, 2013).

CHIRP Profile Overview

Throughout Pyramid Lake, CHIRP lines image two distinct sediment packages marking differences in depositional environment (divider shown in Figs. 4–12 as a red line). Because of varying erosional and tectonic environments throughout the lake, the package tracks at varying depths throughout the profiles. A distinctive, low-amplitude sedimentary package fills the deepest portions of the basin and consistently onlaps onto the older sedimentary packages. Using dating techniques explained in a later section, the distinctive boundary between low-amplitude sediments and more-reflective stratigraphy correlates with the cessation of Tioga glaciation (around 12,500 ka), and a corresponding change in stratigraphic architecture (i.e., changing from more conformal patterns of sedimentation to infilling of lows).

Offset across the Lake Range fault (Fig. 3) is imaged in numerous CHIRP profiles along the eastern edge of the basin (Fig. 4). This north-striking, down-to-the-west fault plays a significant role in the structure of the lake basin due to its size and geometry. In contrast, the Pyramid Lake fault, exposed on land south of the lake, is not directly observed within any of the southern profiles; however, the regional dip of the stratigraphy suggests the presence of a fault to the west (Fig. 5). To the northwest, the basin is characterized by a dramatic increase in the density and change in style of faulting. North- to northwest-striking oblique-slip faults dominate the northern basin. Correlation of many of the faults between CHIRP profiles in the northwest region of the lake is uncertain because the faults are short and segmented relative to line spacing.

Stratal dips observed in the profiles reveal the complicated geology of the Pyramid Lake basin. The changes in dip patterns are annotated in Figure 3. Green profiles indicate west-dipping stratigraphy, and purple highlights an eastern dip, while red shows the locations of more symmetrical profiles. In the southern end of the lake, the lines show a regional southwestward dip of stratigraphy, tilting toward a northeast-dipping Pyramid Lake fault (Fig. 5). The dip suggests that the fault has an extensional component near its northern terminus. To the north, just south of Anaho Island (Fig. 3), the stratigraphy west of the Lake Range fault dips to the east (Fig. 6). Near the middle of the lake, the beds become more symmetrical in dip (Figs. 7 and 8). This symmetrical pattern gives way northward to another area of eastward-dipping beds (Fig. 9) and again transitions into a regime of symmetrical beds at the very north end of the lake (Fig. 10).

The north-south seismic lines show regional changes in dip (Figs. 11 and 12). Figure 11 shows that the laminated sediments beneath the red horizon dip to the south, and this dip decreases toward the center of the basin. The maximum depth of the red horizon occurs just north of the "gas" label (Fig. 11). The north ends of the longer profiles (lines D08L03, D08L04, and D09L01) exhibit a regional gentle dip to the south in the central part of the basin (Fig. 11). In contrast, the strike lines collected along the western lake exhibit a more abrupt change in dip from south to north in a more synformal geometry (Fig. 12). Along the eastern strike lines, the north-dipping slopes are greater than the south-dipping slopes (Fig. 11). Along the western strike lines, the slopes are more equivalent (Fig. 12). A low-amplitude transparent unit mantles the red horizon and infills relief. Note that the alternating dip from west to east observed in the east-west–trending lines is roughly flat. In the north-south–trending lines, these images show the stratigraphic units along their strike (Fig. 3). The low-amplitude package is thicker in the deeper portions of these profiles and onlaps both the northern and southern slopes. In general, the low-amplitude package thickens to the south in all of the north-south–oriented profiles.

Sediment Horizons

The stratigraphic horizons observed in the CHIRP profiles have distinctive patterns throughout the lake. Changes in reflectivity may indicate varying depositional environments. The high-resolution data show a distinctive wavy pattern at shallow depths along profiles toward the eastern shore of the lake. This "hummocky" texture can be observed on the eastern side of the profiles within the southern portion of the lake (Figs. 4 and 5). Two profiles are shown, though nine out of the southernmost 10 profiles include this hummocky texture.

Some areas show a lack of reflectivity from "gas wipeout," where layers cannot be observed or traced across the profile. Small amounts of interstitial gas create an impenetrable layer that limits seismic imaging on profiles

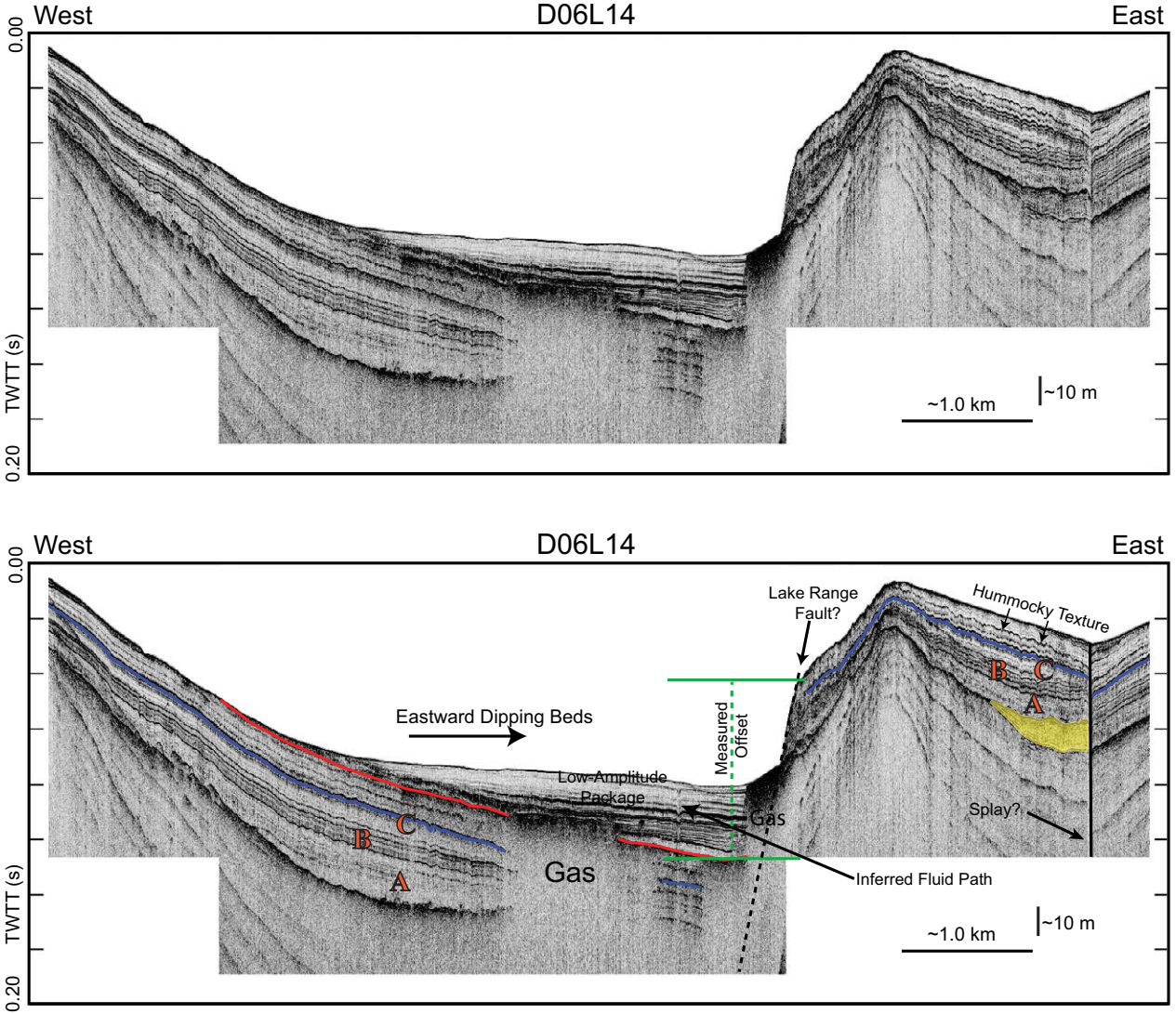

Figure 4. Uninterpreted (top) and interpreted (bottom) compressed high-intensity radar pulse (CHIRP) line D06L14 (for location, see Fig. 3), an east-west–oriented profile acquired across the Lake Range fault, imaging eastward-dipping beds, hummocky texture, gas wipeout, an inferred fluid path, a strike-slip fault on the east end of the profile, and the low-amplitude sediment package with the red horizon. Faults are black lines in the interpreted image. A, B, and C depict a sediment package consisting of ~5–6 laminated reflectors (B) bounded by two transparent layers above (C) and below (A). This package can be observed on both the hanging wall and footwall, as well as traced around the basin. The yellow transparent wedge to the east shows vertical offset that was infilled with sediments at an undeterminable time that cannot be correlated east across the oblique fault. The red and blue horizons correlate to core PLC92B traced from line D07L08 yielding ages of ca. 14 ka and ca. 48 ka, respectively. TWTT—two-way traveltime.

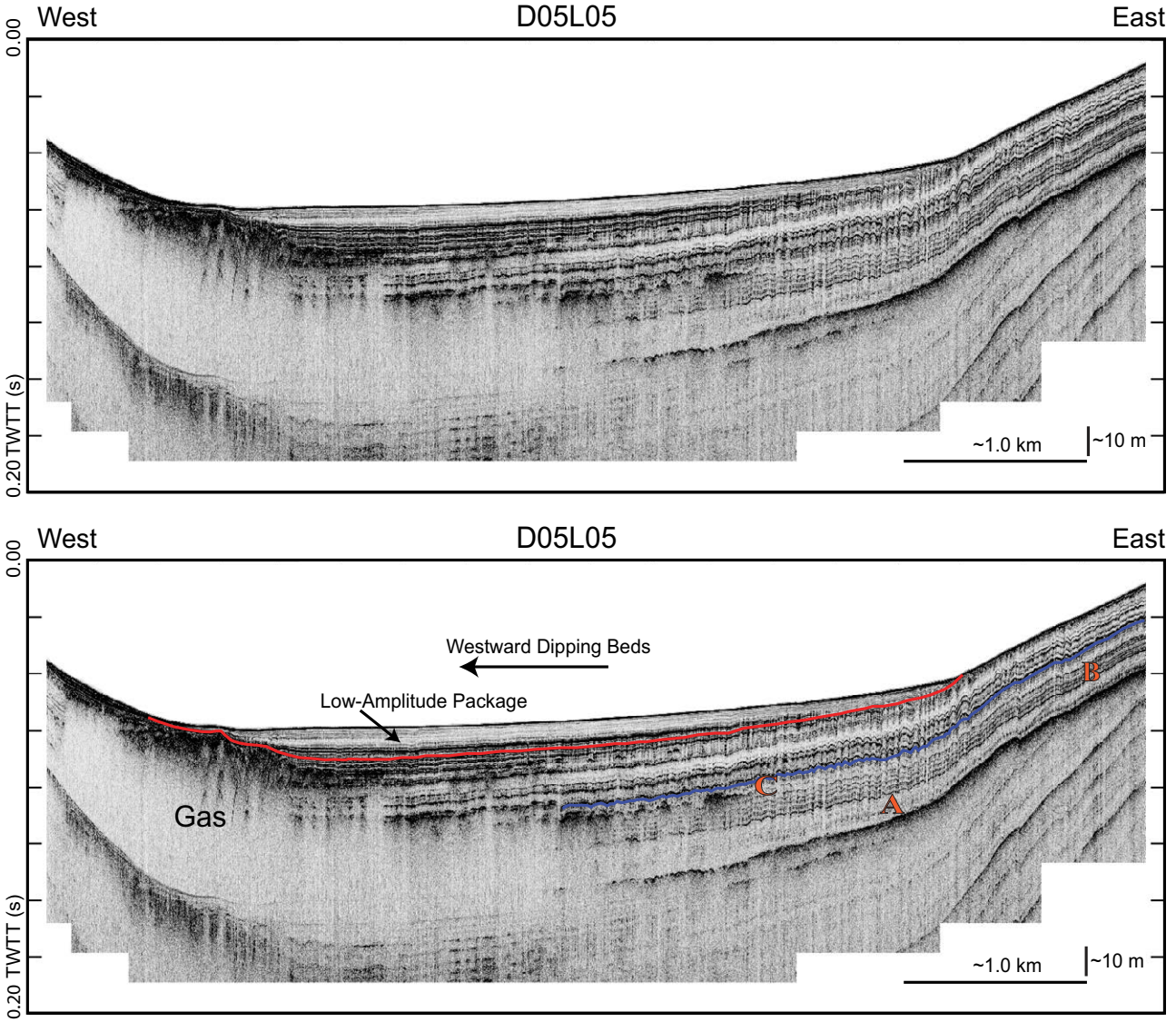

Figure 5. Uninterpreted (top) and interpreted (bottom) compressed high-intensity radar pulse (CHIRP) line D05L05 (for location, see Fig. 3) is a northeast-southwest–oriented profile showing a regional southwestward dip as well as gas wipeout in the west and the low-amplitude sediment package above the red horizon. The red and blue horizons have been correlated throughout the seismic grid (Fig. 3) and to core PLC92B. A, B, and C depict a sediment package consisting of ~5–6 laminated reflectors (B) bounded by two transparent layers above (C) and below (A). TWTT—two-way traveltime.

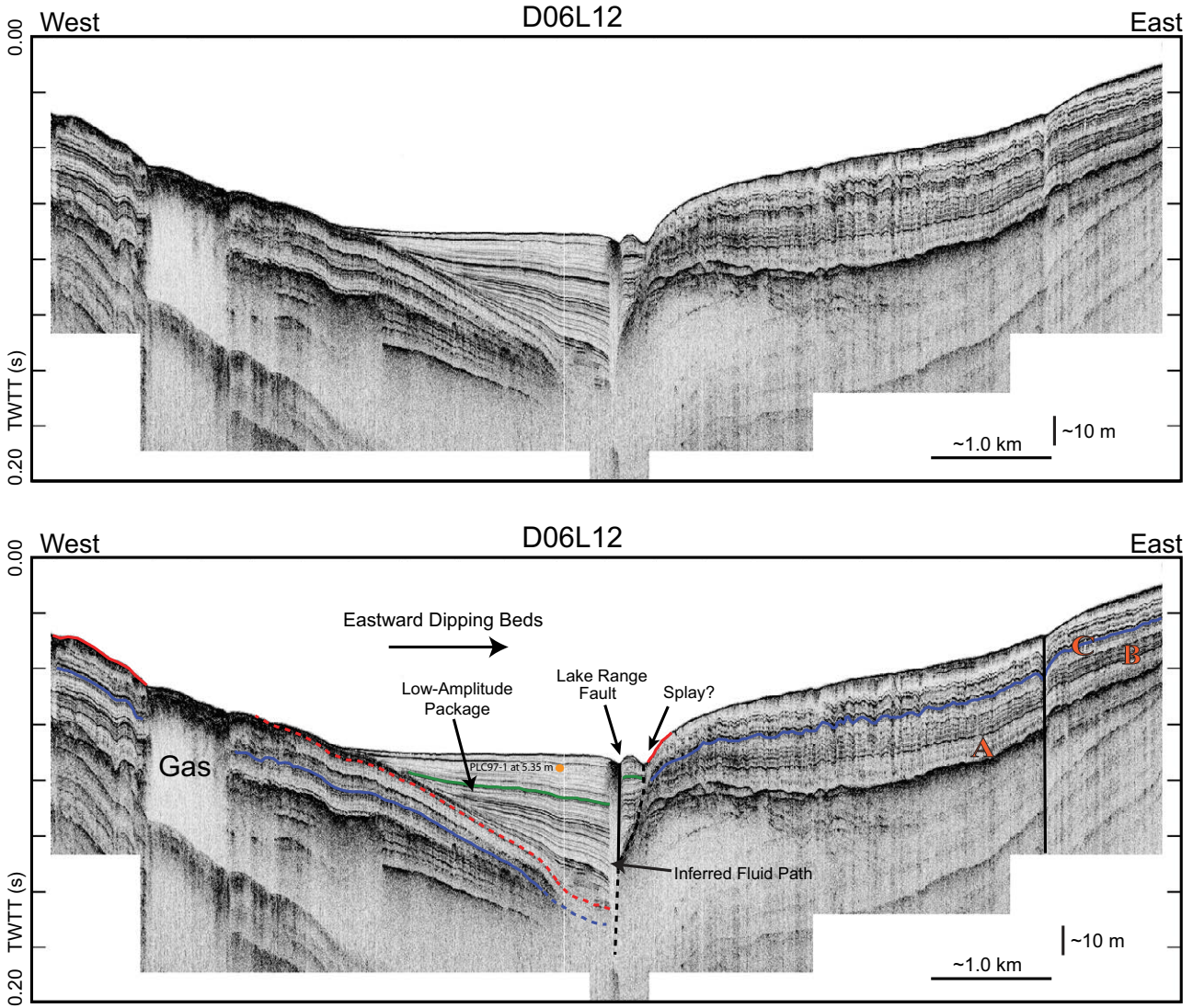

Figure 6. Uninterpreted (top) and interpreted (bottom) compressed high-intensity radar pulse (CHIRP) line D06L12 (for location, see Fig. 3) shows the Lake Range fault and the low-amplitude sediment package infill to the west. It shows distinct eastward-dipping sediment layers. The orange dot correlates to core PLC97-1 traced south to line D06L12. The green horizon is where the offset was measured as well as the extrapolated dates from core PLC97-1. A, B, and C depict a sediment package consisting of ~5–6 laminated reflectors (B) bounded by two transparent layers above (C) and below (A). TWTT—two-way traveltime.

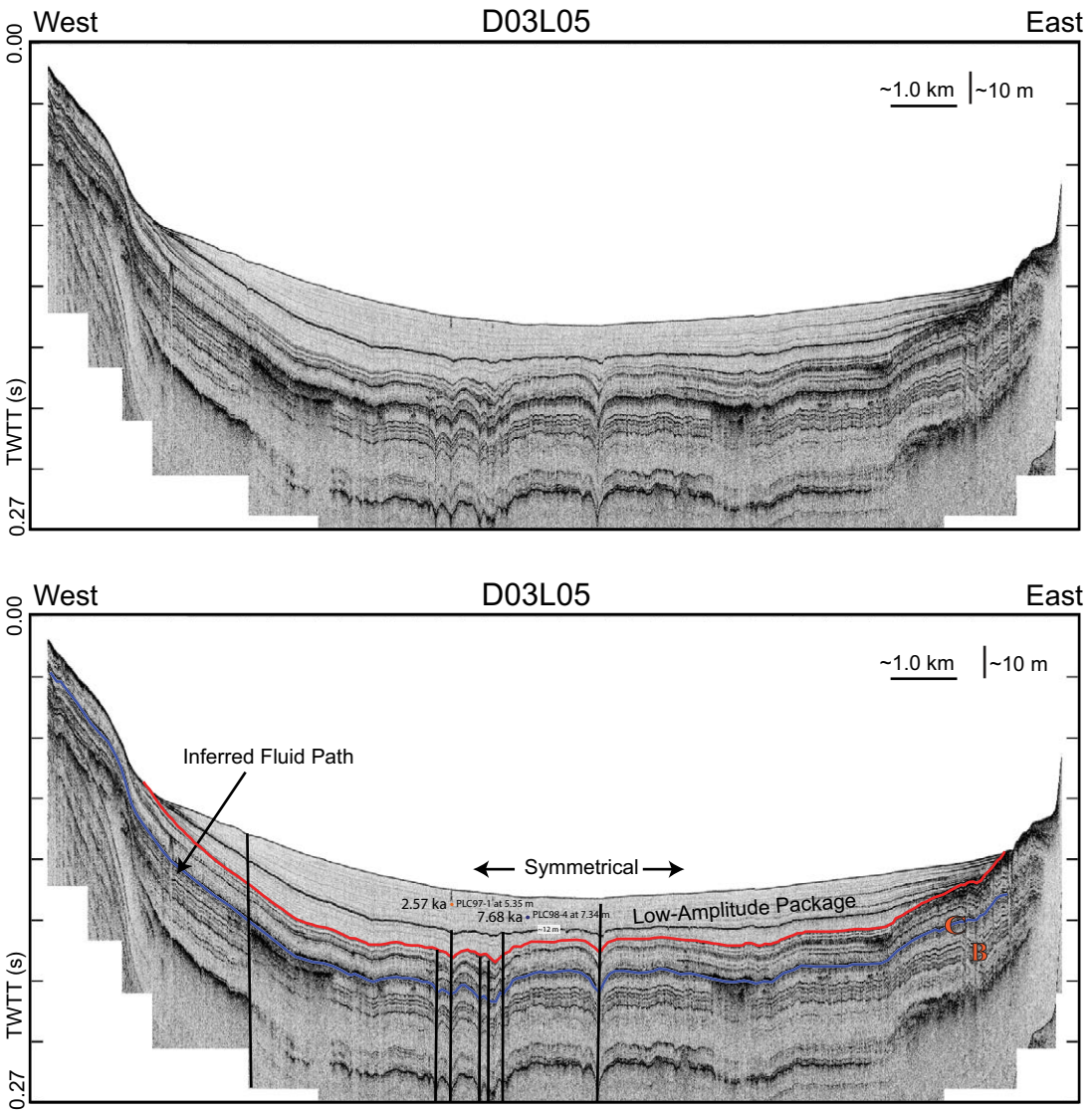

Figure 7. Uninterpreted (top) and interpreted (bottom) compressed high-intensity radar pulse (CHIRP) profile of line D03L05 (for location, see Fig. 3) shows symmetrical beds. It is unclear if the east edge of the profile is the Lake Range fault or the side of the basin, yet numerous other dip-slip faults are present throughout the profile. Gas wipeout and an inferred fluid path are also observed. B and C depict a sediment package consisting of ~5–6 laminated reflectors (B) bounded by a transparent layer above (C). TWTT—two-way traveltime.

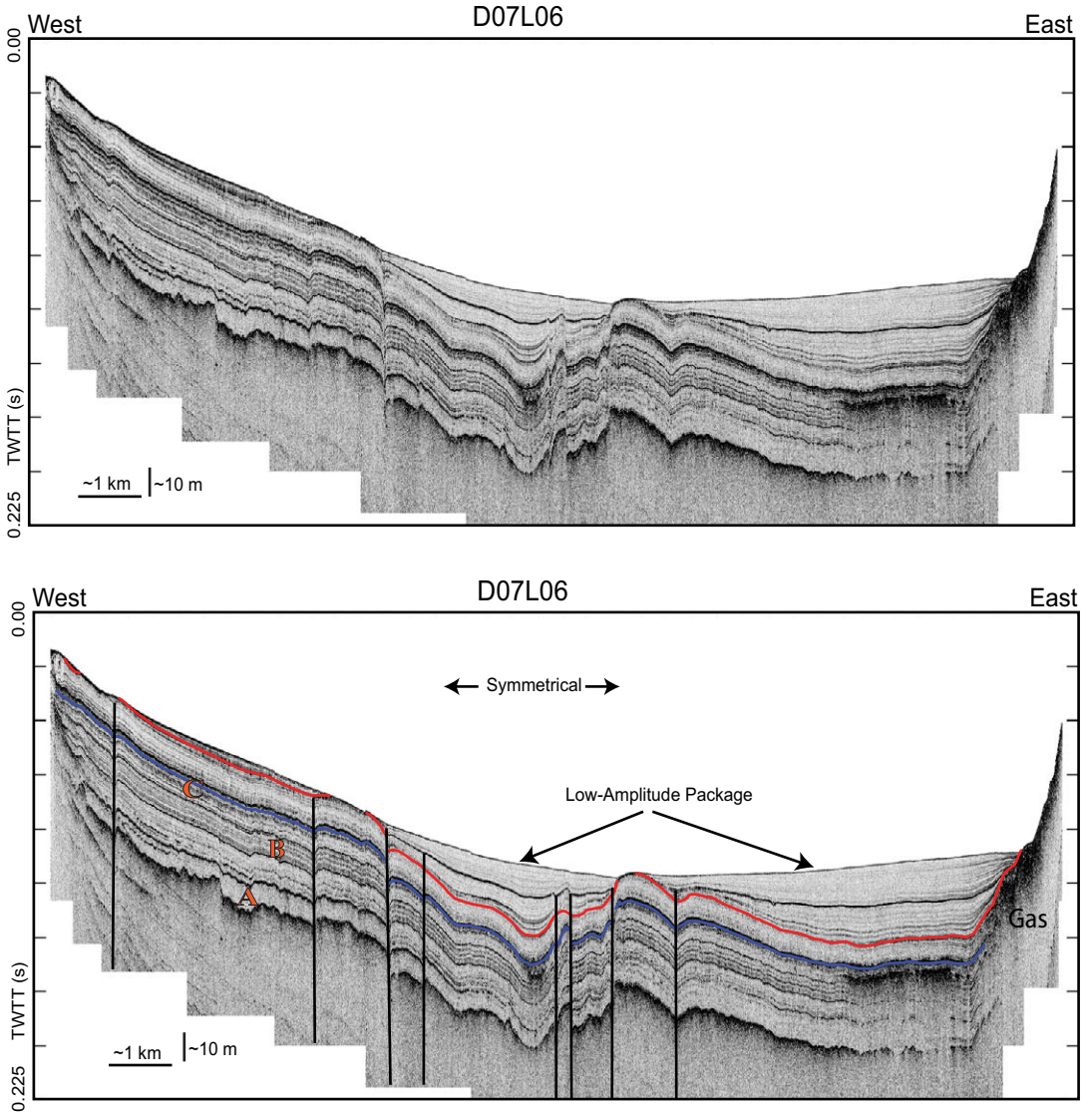

Figure 8. Uninterpreted (top) and interpreted (bottom) compressed high-intensity radar pulse (CHIRP) profile of line D07L06 (for location, see Fig. 3) shows eastward-dipping beds to the west and symmetrical beds to the east as well as the onset of the northwest fault network. The low-amplitude package is thick in this region, gas is present to the east, and the Lake Range fault appears to be just east of the profile. A, B, and C depict a sediment package consisting of ~5–6 laminated reflectors (B) bounded by two transparent layers above (C) and below (A). TWTT—two-way traveltime.

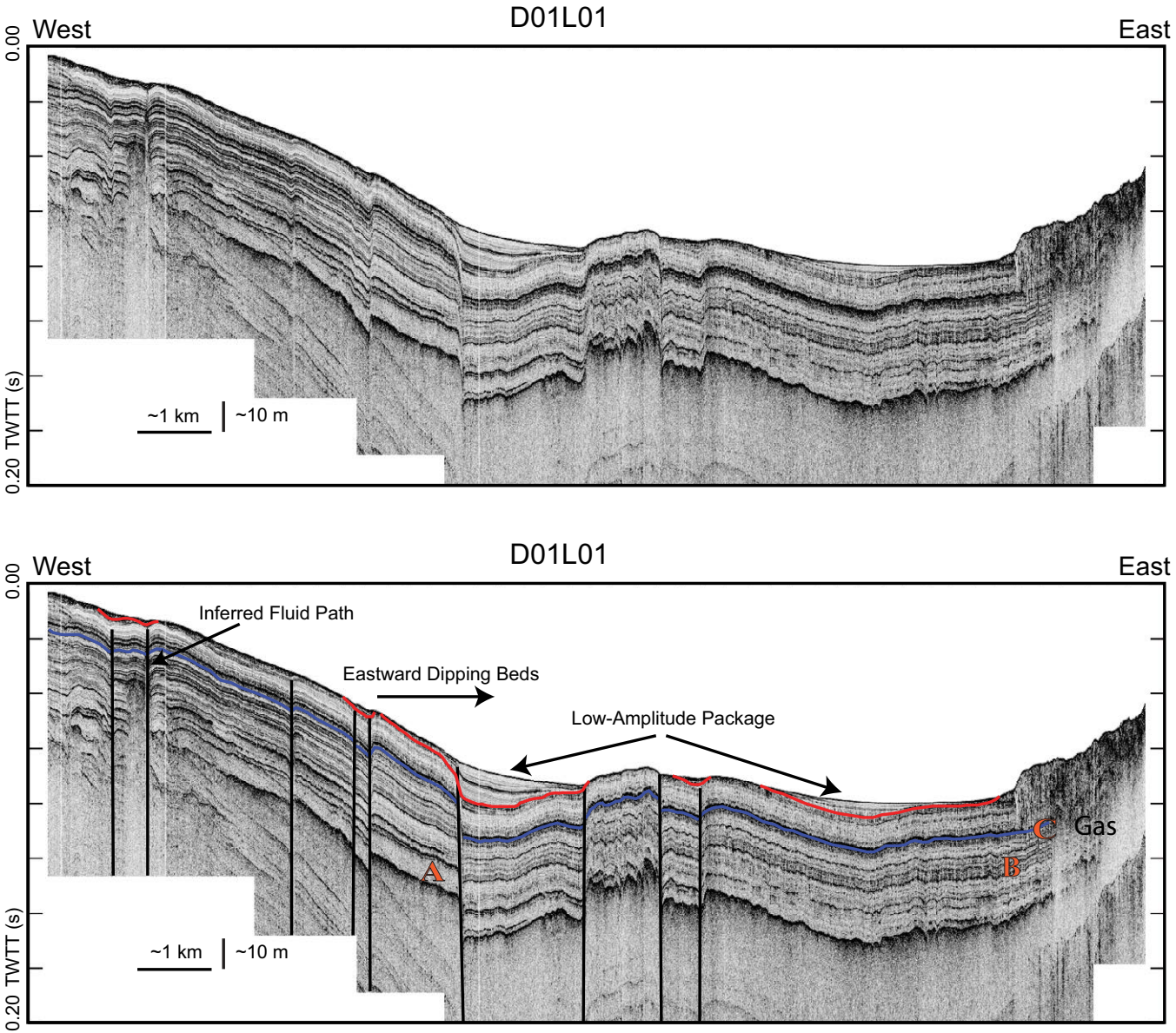

Figure 9. Uninterpreted (top) and interpreted (bottom) compressed high-intensity radar pulse (CHIRP) line D01L01 (for location, see Fig. 3) shows an increased number of distributed faults toward the northern portion of the basin (as opposed to Figs. 4–7). There is also a noticeable eastward dip of the beds. A, B, and C depict a sediment package consisting of ~5–6 laminated reflectors (B) bounded by two transparent layers above (C) and below (A). TWTT—two-way traveltime.

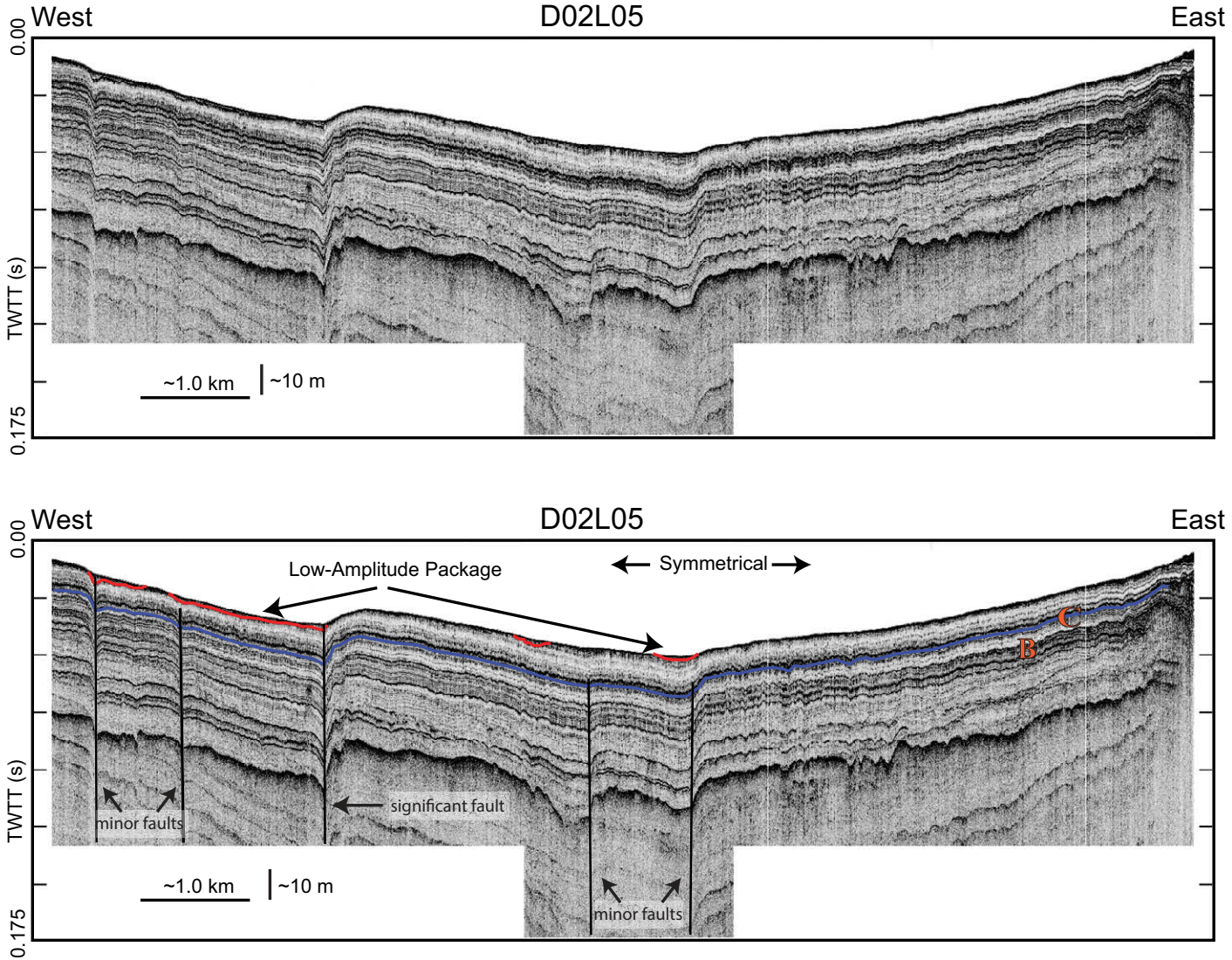

Figure 10. Uninterpreted (top) and interpreted (bottom) compressed high-intensity radar pulse (CHIRP) line D02L05 (for location, see Fig. 3) reveals that the northernmost profiles have a symmetrical structure. The low-amplitude package is barely observed this far north. B and C depict a sediment package consisting of ~5–6 laminated reflectors (B) bounded by a transparent layer above (C). TWTT—two-way traveltime.

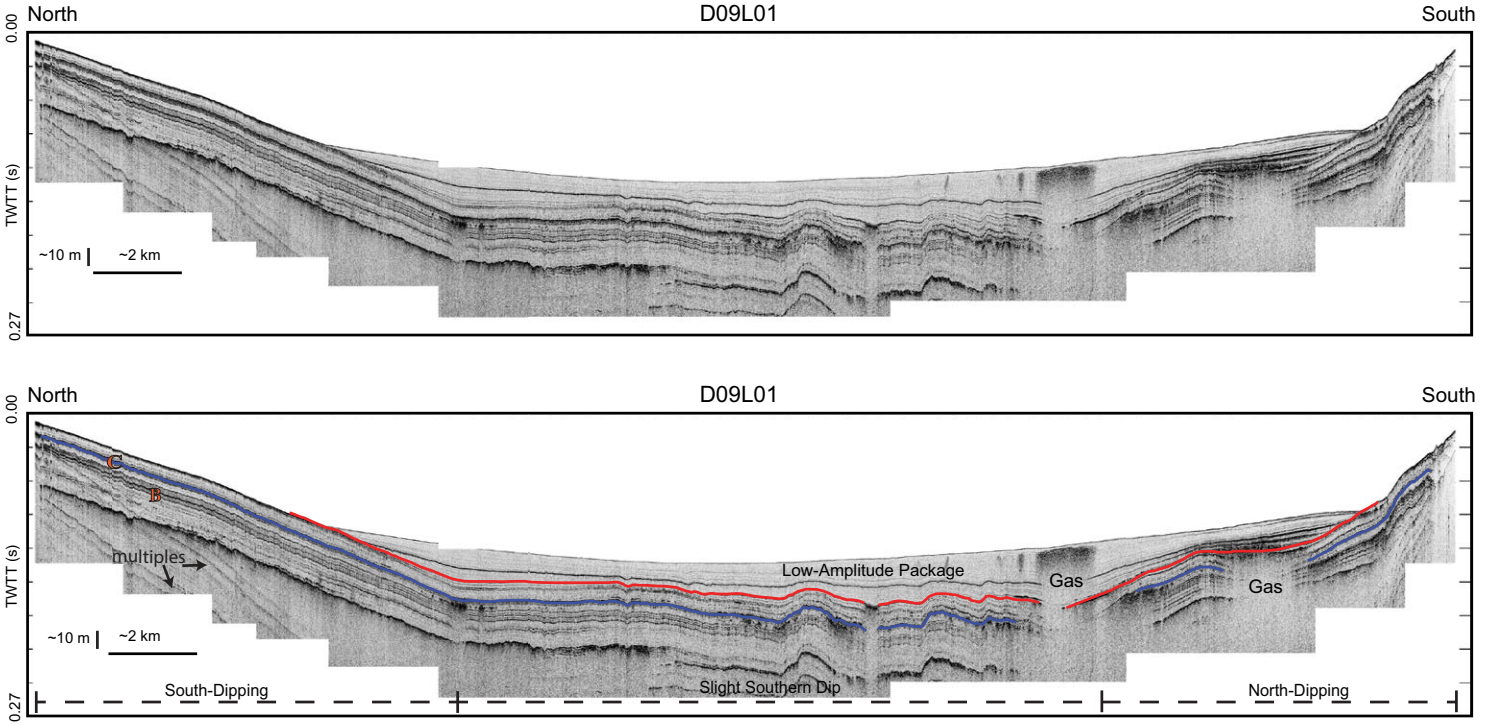

Figure 11. Uninterpreted (top) and interpreted (bottom) compressed high-intensity radar pulse (CHIRP) line D09L01 is a north-south–oriented line located on the eastern edge of the basin (see Fig. 3). It shows the thickness of the low-amplitude package systematically increasing to the south. B and C depict a sediment package consisting of ~5–6 laminated reflectors (B) bounded by a transparent layer above (C). TWTT—two-way traveltime.

throughout the lake (e.g., Figs. 4 and 5). This gas is typically due to biogenic breakdown or some similar process in the shallow sediments. These gas zones tend to block the acoustic energy over a horizontal distance rather than along a narrow column. Fluid flow also causes a type of "wipeout," where imaging is limited, but those regions are narrowly confined and typically collocated near faults (e.g., Fig. 4). In the panhandle region of the lake, all northeast-southwest lines have "gas wipeout" toward the west, with the exception of the northernmost line D06L10 (location shown in Fig. 3). Farther north, the east-west lines show "gas wipeout" along the eastern margin of the basin with few exceptions. The acoustic wipeout in these areas seems to be correlated with the greatest asymmetries in stratal dips and basin architecture. Lines D07L02, D01L01, and D09L02 (locations shown in Fig. 3) suffer from gas wipeout only along the western edge. All of the northwest-southeast and north-south profiles experience gas wipeout either near the edges of the lines or along the faults themselves. Lines D02L11, D02L07, D02L05, and D07L10 are the only lines in the lake without any notable acoustic blanking.

Twelve of the lines show narrowly confined regions were reflectivity is disrupted near a fault or other planar feature (Figs. 4, 6, 7, and 9). Interpretations of these profiles suggest that the paths indicate fluid flow through the shallow sediments. These fluid paths do not always reach the lakebed; rather, some of these features appear to be capped by stratigraphic horizons at various depths (e.g., Fig. 7). Most profiles contain only one fluid pathway; however, line D06L08 has a maximum number of 11 fluid paths, and line D06L01 has five fluid paths scattered throughout. These features are observed near fault planes, highlighting the way that faults serve as fluid conduits in the Pyramid Lake basin.

A change in depositional style is widely observed within the deepest portion of the basin, visible as a transparent (low-amplitude) region above a highly reflective horizon (annotated in red in Figs. 4–12). The age of this horizon (discussed further in a later section) is identified as the Pleistocene-Holocene boundary, ca. 12 ka. The layer is mostly observed in the deeper portions of the lake, although small isolated lows along the slopes are also infilled, and the infilling stratigraphy onlaps onto the older units (e.g., Fig. 8). The thickness of the

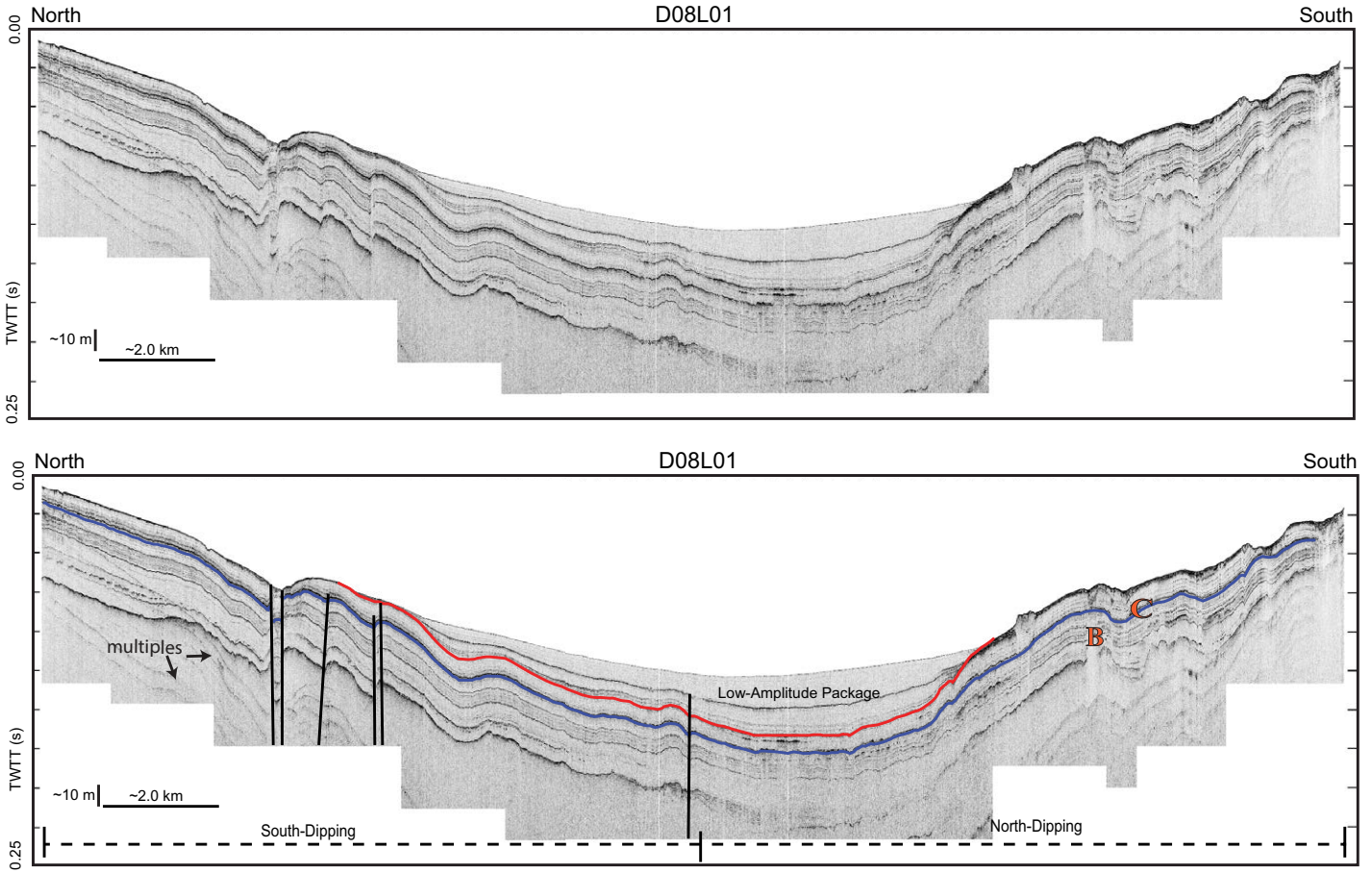

Figure 12. Uninterpreted (top) and interpreted (bottom) compressed high-intensity radar pulse (CHIRP) line D08L01 is a north-south–oriented profile located on the western side of the basin (see Fig. 3 for location). This profile shows the north end of the basin dipping south and the south end dipping north with the low-amplitude sediment package thickening to the south. B and C depict a sediment package consisting of ~5–6 laminated reflectors (B) bounded by a transparent layer above (C). TWTT—two-way traveltime.

low-amplitude package varies depending on profile and its location. In the panhandle lines (southern basin), the sediments within this package have limited thickness; however, they spread horizontally along most of the lake bottom (Fig. 5). At line D05L14 (location shown in Fig. 3), the structure of the low-amplitude package drastically changes as sediments become east dipping near the eastern edge of the basin. This profile is similar in appearance to lines D06L12 (Fig. 6) and D06L14 (Fig. 4). The low-amplitude/nonreflective sediments onlap layers toward the western side of the lake and diverge toward the eastern portion of the lake (i.e., Figs. 4 and 6). In the central part of the basin, the low-amplitude package is much thicker in comparison to the southern profiles (Fig. 8). Though thinner in the south, the divergent wedge stretches across the entire basin floor and is not localized near the fault (Fig. 5). Toward the north end of the lake, the low-amplitude package becomes thinner and is not present in the shallower water of the two most northern lines (northern end of Figs. 11 and 12).

An additional set of sediment packages is observed in the CHIRP profiles. The horizons show consistent reflectivity patterns across the lake and can be acoustically correlated across fault offsets. Line D06L14 (Fig. 4) shows the three sets of layers highlighted by A, B, and C on both the hanging wall and

footwall of the Lake Range fault. This package consists a laminated section of sediment (B) enclosed between two transparent stratigraphy sections above (C) and below (A). The laminated section consists of approximately five to six reflectors. These horizons record the offset across faults in numerous portions of the lake.

Core Data

The ages of stratigraphic units are inferred from sediment cores and derivative products collected for paleoclimatic studies by Mensing et al. (2004), Benson et al. (2002), and Benson et al. (2013). The age controls on the cored units have been projected onto relevant seismic sections for dating stratigraphic horizons and correlating dates. The five cores that were used in this study are PLC97-1, PLC98-4, PLC08-1, PLC92B, and PLC97-3 (locations in Fig. 3). Ages and depths of cores are chronicled as follows. Piston core PLC97-1 penetrates to a depth of 5.35 m. Age control is based on paleomagnetic secular variation (PSV) and radiocarbon ages on total organic carbon (TOC), where the top of the core is dated at 105 ± 50 yr (using ^{14}C), while the core bottom dates to 2.57 ka. Piston core PLC98-4 recovered 6.34 m of sediment, with ^{14}C chronologic dates spanning from 3.98 ka to 7.69 ka. PLC08-1 reached a depth of 16.78 m, and age controls from $\delta^{18}O$, total inorganic carbon (TIC), and PSV measurements place the top sediment layer at 15 ka (using Greenland Ice Sheet Project [GISP2] age) and the bottom at 49.3 ka. PLC92B was cored to 17.32 m, and $\delta^{18}O$, $\delta^{13}C$, total carbon (TC), and TIC date the top of the core at 13.9 ka (GISP2 age) and the bottom at 47.9 ka. The last core, PLC97-3, used the same age controls as PLC92B, cored to 3.52 m, and dated the top layer at 11.7 ka and the bottom age either at 17.5 ka or, using ^{14}C measurements, at 15.5 ka.

Pyramid Lake Fault Network

Lake Range Fault

The architecture of the Pyramid Lake basin is predominantly controlled by a large normal fault running along the eastern edge of the lake. This down-to-the-west normal fault is imaged and measured in nine profiles (and possibly three more) in the middle section of the lake basin. The Lake Range fault is bounded from line D05L14 through line D03L05 (locations shown in Fig. 3), with the one exception of line D07L02, where the majority of slip is likely located onshore. The measured vertical offset (direct and apparent) ranges between 25 m (i.e., green horizon in Fig. 6) and 113 m (labeled in Fig. 4). Tracking the fault offsets between profiles shows numerous areas where the fault likely splits into multiple splays or fault segments. This segmentation on the Lake Range fault provides insight into how the fault potentially splays onto land or represents a more continuous fault that is strongly segmented by slip rate.

Perhaps one of the most remarkable demonstrations of the Lake Range fault is observed in line D06L12 (Fig. 6) The high-angle (measured at ~60° in CHIRP images), west-dipping normal fault is located about halfway through the CHIRP line and has a maximum measured offset of ~32 m. Chronostratigraphic correlations through core data (discussed in a later section) suggest that most of this motion has occurred within the Pleistocene.

The Lake Range fault appears to be segmented throughout the lake basin. Alternating stratigraphic patterns (denoted by colors in Fig. 3) show areas of symmetry and asymmetry that are expressed through changes in the way in which the layers dip in the lake. The dipping layers are influenced by lake bathymetry (i.e., erosion and climatic change) and also through tectonic motion of the Pyramid Lake fault (Fig. 5) and the Lake Range fault (i.e., Fig. 6). The most southern expression of the Lake Range fault lies just south of Anaho Island. Line D05L12 shows a small amount of down-to-the west offset. Directly north on lines D05L14 and D06L12 (Fig. 6), a significant amount of vertical deformation is imaged (profile locations shown in Fig. 3). The observed eastern divergence changes dramatically over a very short space, showing that fault offset has accumulated over a very short spatial scale.

Pyramid Lake Fault

The dextral strike-slip Pyramid Lake fault is observed on land though geologic mapping near the southwestern shore. The fault is hypothesized to continue into the lake along the southwest corner of Pyramid Lake (Drakos, 2007; Faulds and Henry, 2008; Faulds et al., 2005b; Anderson and Hawkins, 1984). The CHIRP images do not image any large strike-slip fault entering the southern end of the lake, though the presence of the Pyramid Lake fault is indicated by the sharp linear nature of the southwestern shoreline along the panhandle. Profiles within the panhandle of the lake show southwestward-dipping stratigraphy (Fig. 5).

Northwest Fault Network

The number and density of both significant and minor faults (depending on fault extent and observed offset; i.e., Fig. 10) within the lake basin change considerably near the northern end of the lake (Figs. 3, 8, and 9). Profiles near the southern end (lines D05L03–D07L04) generally have two to five minor faults per line (Fig. 3). Profiles to the north (lines D07L06–D02L05) have between seven and nine faults per profile. The two northernmost lines do not contain any noticeable faults. The faults are traced between profiles and show a north-northwest and northeast strike. More strike-slip–dominated faults are visible where layers dip or collapse into the fault plane in a symmetric fashion, forming a "V" in the stratigraphic pattern. The combination of vertical offset with a "V" near the fault plane implies some element of oblique motion on the fault segment. Compared to the Lake Range fault, these faults have significantly less vertical throw and less along-strike continuity.

DISCUSSION

Stratigraphic patterns observed in the CHIRP profiles provide an improved understanding of the fault architecture beneath the lake. The stratigraphy also allows identification of a cluster of offset events in the Holocene due to the motion that is observed across the ca. 9.5 ka horizon (green in Fig. 6). By correlating stratigraphic layers to sediment cores, vertical slip rates can be calculated across faults. Understanding the rates of motion on these large, active fault systems and their recurrence interval has important implications to assessing earthquake hazards for northern Nevada and the Reno metropolitan area.

Polarity Flip and Fault Segmentation in Pyramid Lake

One of the most prominent features observed in the CHIRP profiles is an alternating pattern of dip directions within the sedimentary layers (Fig. 3). Most notably, the stratigraphy highlights a flip in basin polarity near Anaho Island. Sediment layers tilt and thicken toward normal faults, similar to what is imaged in other extensional settings (Bosworth, 1985; Flannery and Rosendahl, 1990; Rosendahl et al., 1992; Driscoll et al., 1995; Brothers et al., 2009). The alternating dips show where fault motion dies on one fault segment and steps to another segment.

Results indicate that the Pyramid Lake fault enters the basin along the southwestern shoreline of the lake (along the panhandle). The fault is not directly seen in the CHIRP profiles nor is it observed on land through geological mapping adjacent to the lake, though the effects of the fault are seen from the western sediment dip in the southern basin (i.e., Fig. 5). By defining the western shore, there is no surface expression to be mapped, and CHIRP profiles were not able to cross the fault trace to image the fault directly. Insight about the location and the sense of motion on the Pyramid Lake fault can be inferred from the four southernmost profiles that run perpendicular to the southwestern shore. These profiles display a regional southwestward dip (divergence) in stratigraphy (e.g., Fig. 5). This divergent pattern suggests that the Pyramid Lake fault has a northeast-dipping, normal component near its northern termination. The fault slip changes to oblique motion at its end and transfers strain (steps over) onto the Lake Range fault. Oblique motion on the Pyramid Lake fault would help to form the "accommodation" that is the southern basin/panhandle. The impact that this motion has on the morphology of the lake bottom gives strong evidence that the fault extends along the western shoreline of the panhandle (Fig. 3).

Farther north, profiles reveal the transfer of motion from the Pyramid Lake fault onto the Lake Range fault. The stratigraphic pattern changes to a regional eastward dip near Anaho Island rather than the westward dip south of Anaho Island, where motion on the Pyramid Lake fault dominates. The transition between the northern termination of the Pyramid Lake fault and the beginning of the Lake Range fault is observed between line D05L12 and line D05L14 (locations shown in Fig. 3). Between the two profiles, the stratigraphic horizons change from a western dip to an eastern dip. The Lake Range fault dominates the architecture of the basin north of Anaho Island and controls stratigraphic patterns along the eastern shoreline (Fig. 3). Stratal relationships suggest that the initiation of the Lake Range fault evokes a flip in the stratal dip caused by the west-dipping Lake Range fault (Flannery and Rosendahl, 1990; Bosworth, 1985; Rosendahl et al., 1992).

The pattern of regional eastern dip oscillates into segments that are more symmetric (these regions are color-coded in Fig. 3). This change between symmetrical and asymmetrical architecture provides evidence for fault segmentation along the Lake Range fault. Slip on the Lake Range fault dominates in regions that have a strong eastward dip. These regions show where the stratigraphic horizons tilt and thicken into an extensional, west-dipping fault zone (Fig. 6). Regions with more symmetric horizons (i.e., Fig. 7) show where strain is not focused or decreases on the Lake Range fault. There are two options to explain this alternating pattern of symmetry/asymmetry. One explanation invokes strong segmentation along the strike of the Lake Range fault with splays that occasionally trend onshore, striking north to northeast, away from the main trace. In this mode, slip is somewhat constant along strike, but dip is controlled by the relative distance of the fault from the shoreline. Otherwise, fault segmentation may genuinely represent strong gradients in slip along the fault trace, with little or no "horse-tailing" onshore. In reality, it may be a hybrid model, where segmentation is supported through onshore splays, but also by changes in cumulative offset along strike.

The change in deformation style from the south to the north is evidence of both an architectural change in basin polarity and strong segmentation of the Lake Range fault. Broadly speaking, sediment layers south of Anaho Island dip west (or southwest), while layers north of the island dip toward the east. This change in deformation corresponds to a change in basin geometry. South of Anaho Island (i.e., the panhandle), the basin is narrow and oriented northwest, whereas north of the island the basin, fans open or widen and trend north-south. This latter pattern reflects a combination of the north-striking Lake Range fault and a series of northeast-striking oblique-slip faults.

Pyramid Lake Fault Patterns

Predominantly transtensional faulting is observed in CHIRP data in the northwest end of the Pyramid Lake basin near the Needles (Figs. 3 and 9). This is a different deformational style than the rest of the lake, as the density of oblique-slip faults markedly increases, but the overall length of these faults decreases. The faults in the northern end of the lake are 2–10 km long, barely crossing two east-west–oriented CHIRP lines. These short, segmented faults are very suggestive of a developing shear zone (Wesnousky, 2005a). Conversely, the Lake Range fault, which is continuous for >20 km along the eastern shoreline of the lake (Fig. 3), shows a slight westward dip on profiles (i.e., Fig. 5), suggesting that this region inherits a component of northeast-dipping normal slip before terminating near Anaho Island.

Many of the faults imaged in the profiles in the northern portion of the lake show signatures of strike-slip deformation in addition to their obvious vertical offsets (Fig. 9). Strike-slips faults are identified from two-dimensional sections in seismic stratigraphy through a "V" signature, where layers dip in toward a fault plane. This signature is due to small amounts of transtension on the fault plane that allow the sediment layers to collapse toward the fault. The significant faults documented in the northwest edge of the basin appear to be a suite of north- to northwest-striking oblique faults and northeast-striking oblique-slip faults. This transtensional faulting forms the "fan" shape of the northern basin (Fig. 3). Unlike the more mature Lake Range fault and Pyramid Lake fault, the shorter faults imply that the northern basin is an immature system that has yet to coalesce into a single continuous fault (Faulds and Henry, 2008).

The southern portion of Pyramid Lake displays wavy stratigraphy on the eastern side of a number of profiles (i.e., Fig. 4). Close inspection shows distinct breaks in stratigraphic continuity that may be due to downslope, earthquake-induced sliding or some other deformation process.

Stratigraphy and Cores

By correlating the stratigraphy observed in the high-resolution CHIRP data with core data from Mensing et al. (2004), Benson et al. (2002), and Benson et al. (2013), it is possible to constrain vertical slip history within the basin. There is a depth-age distribution of sediments within Pyramid Lake attributed to the erosion and reworking/resuspension of older sediments from the sides of the basin that was well known from coring before CHIRP profiles were collected (Benson et al., 2002). The ages of the sediments along the edges of the basin are much older than the deep, middle section of the lake (Benson et al., 2002). This age unconformity is seen in the CHIRP data and highlights a depositional hiatus. The horizon may mark different styles of deposition: During periods of glaciation, sediment may, on average, have been finer grained, and deposition was hypopycnal, and this created a pattern of sedimentation that mimics topography. Holocene deposition was hyperpycnal, as it consisted of much coarser material that bypassed the shallows and steep slopes, infilling the deepest sections of the basin, mostly fed by the nearby Truckee River delta at the south end of the lake.

Using chronologic control from sediment cores and the high-fidelity stratigraphic record observed in the CHIRP profiles, sediment layers can be correlated across the faults throughout the basin with a high level of confidence. Correlation of the sediment ages with the horizons of vertical offsets allows (in some cases) the vertical slip rate (vertical throw rate) to be calculated across several of the more significant faults (Table 1; black dots in Fig. 3). Core PLC92B was dated using the GISP2 age, with the top dated at 13.9 ka and the bottom, at a depth of 17.325 m, showing an age of 47.9 ka (Benson et al., 2013). This core is located at the west end of line D07L08 just to the north of the profile (Fig. 3). The horizons that bound the top and bottom of the core were correlated with the nearest stratigraphic horizon and then traced south (using Fledermaus and Kingdom Suite) around the basin to the Lake Range fault on line D06L12 (Fig. 6) to constrain the long-term slip rate and reconstruct the slip history. These layers represent the layers recorded in core data that can be used to date CHIRP horizons (Fig. 13). The red horizon marks a change in deposition to the low-amplitude package. Dates support the interpretation that the low-amplitude package is Holocene in age and was deposited after the last glaciation (Tioga) around 12,500 yr ago.

The long-term slip history of the Lake Range fault is not documented, but given the size of the fault escarpment and depth of the basin, it has likely been

TABLE 1. DISTRIBUTION OF SLIP RATES ON SIGNIFICANT FAULTS WITHIN PYRAMID LAKE

Fault	Line	Slip rate (mm/yr)
f1	D02L05	0.1
	D02L07	0.1
	D02L11	0.1
	D02L01	0.27
	D07L08	0.14
	D07L06	0.18
f2	D02L05	0.11
	D02L07	0.31
	D02L11	0.3
	D01L01	0.17
	D07L08	0.35
	D07L06	0.16
f3	D07L04	0.13
f4	D01L01	0.1
f5	D02L11	0.13
	D01L01	0.11
f6	D02L05	0.13
	D02L07	0.07
f7	D03L03	0.4
	D03L01	0.1
	D06L05	0.3
f8	D06L01	0.19
f9	D06L14	1.5
	D06L12	1
	D05L10	0.2

Note: Vertical component of Holocene slip rate was calculated from various locations in Pyramid Lake (positions illustrated as black circles on Fig. 3). The dense network of profiles allowed the correlation of the 48 ka horizon in several locations across one fault. The range of slip varies from 0.2 mm/yr to 1.5 mm/yr. On the Lake Range fault, slip increases in northern Pyramid Lake area, with very low vertical rates on the southern tip. The faults in the northern portion of the lake vary slightly along strike.

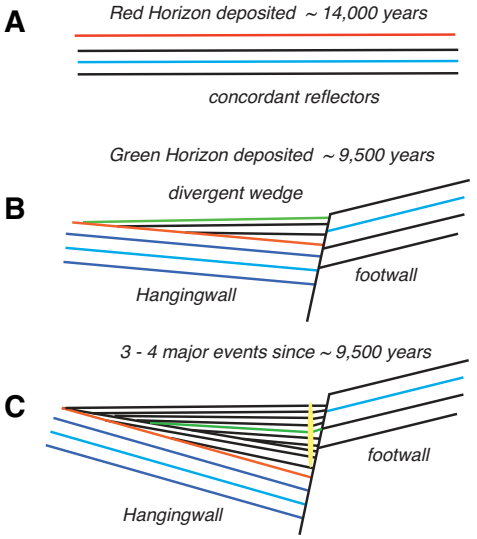

Figure 13. Schematic diagram of the recent tectonic history of the Lake Range fault as observed from line D06L12 (Fig. 4). (A) An inrush of sediments, represented as the blue lines, was deposited before the red horizon. The red horizon was deposited ca. 14 ka in concordant layers. (B) Between ca. 14 ka and ca. 9.5 ka, more sediment layers were deposited, which widened into the fault plane, creating the divergent wedge. The green horizon was deposited ca. 9.5 ka. (C) More layers were deposited above the green horizon, though they are unable to be correlated across the fault splay, likely due to erosion in the footwall block. By assuming a characteristic rupture of 2–2.5 m, three to four major earthquakes occurred after the green line was deposited ca. 9.5 ka. Evidence of the cumulative rupture history is preserved in the divergent wedge, though single events are not discernible. The yellow oval represents a fluid path near the fault plane.

active for the entire Pleistocene and perhaps well into the Pliocene. Near the southern terminus of the fault (Fig. 6), there was vertical displacement across the fault and an infilling of sediments into a low (ca. 14 ka; Fig. 13A). After the red horizon was deposited (ca. 14 ka), the Lake Range fault experienced modest thickening of sediments into the hanging wall near the fault. The thickening (showing vertical offset) is not resolvable to one or possibly numerous events. After the sediment infilling (and most likely correlated with melting glaciers in the Tahoe Basin), many more stratigraphic horizons were deposited into the existing low topography. Little to no differential slip is recorded across these concordant layers within this interval (Fig. 13B).

After the thick wedge of sediments was deposited (Figs. 6 and 13B), significant vertical offset on the Lake Range fault is recorded in the stratigraphy. This series of events allows for the quantitative amount of offset to be calculated, although per-event slip can only be inferred (the blue lines in Fig. 13C). The orange dot in Figure 6 shows the bottom location of core PLC97-1, with an age date of 2.57 ka at 5.35 m (Mensing et al., 2004) that correlates with upper reflectors in the low-amplitude package in line D06L12. The age of the green horizon was extrapolated from this core date in the center of the lake (Fig. 3) by assuming a constant sedimentation rate from the lakebed to the green horizon. This assumption gives an age of ca. 9.5 ka for the green horizon. The time difference between the green and red horizons (Fig. 6) provides a sedimentation rate of 0.17 cm/yr for the past 9500 yr. Published sedimentation rates of ~0.12–0.23 cm/yr for the past 7630 yr (Benson et al., 2002) are consistent with this calculation.

Using the dated horizons from the middle of the basin (core PLC97-1) extrapolated to seismic profile horizons, dates were calculated for the red horizon to be 30.7 ka, while a core along the western edge (core PLC92B) placed the red horizon at 13.9 ka. The two different age calculations imply 16,000 yr of "missing" sediment. This discrepancy of ages on the red horizon likely indicates a short interval of enhanced sedimentation that infilled the low topography near PLC97-1 during melting of Pleistocene glaciers.

Sedimentation continued above the green horizon (blue in Fig. 13C), showing significant slip focused on the Lake Range fault. Though the fault is not directly imaged due to fluid wipeout, the sediment package (the blue horizons and the one green horizon in Fig. 13C) indicates three to four major earthquake events (assuming a characteristic earthquake of 2–2.5 m of vertical throw; Schwartz and Coppersmith, 1984). In total, ~9 m of stratigraphic offset have occurred since the deposition of the green horizon ca. 9.5 ka. Layers above the green horizon cannot be reliably correlated across the Lake Range fault, making the 9.5 ka marker the last reference point for deformation.

Restoring (or collapsing) offset horizons in the seismic stratigraphy allows the measurement of growth on the fault system. Collapsing the low-amplitude package across the fault trace shows that most of the slip occurred after the deposition of the green horizon (i.e., in the past ~9.5 k.y.). Little to no apparent offset is seen below the green horizon, suggesting that all of the tracked horizons (in the "wedge") were deposited before any significant vertical offset occurred—thus, it appears all the slip has occurred since ca. 9.5 ka.

In summary, a high influx of sediment occurred between 12,500 and 9500 yr ago due to the end of the Tioga glaciation. A drastic increase of high Sierra Nevada meltwaters brought a surge of sediment into the lake basin. During this time, there was limited to no tectonic activity on the Lake Range fault. In the past 9500 yr, however, there has been significant offset on the Lake Range fault.

Lake Range Fault Slip Rate

The recent vertical slip rate calculated on the Lake Range fault along three profiles is consistent with other Holocene slip rates in the northern Walker Lane belt. The age inferred for the green horizon (ca. 9.5 ka) and the total offset

seen across the fault (~9.5 m; Fig. 6) yield vertical Holocene slips rate between 0.2 mm/yr and 1.5 mm/yr (Table 1). The West Tahoe and Stateline–North Tahoe faults (Fig. 2) have a normal slip rate of 0.7–0.8 and 0.60 mm/yr, respectively (Kent et al., 2005; Dingler et al., 2009). The Genoa fault has a reported Holocene slip rate of ~2–3 mm/yr, although longer-term rates are closer to 1 mm/yr (Ramelli et al., 1999). Recent seismic work in Walker Lake constrains the slip on the Wassuk fault to be as much as 1.0–1.5 mm/yr over the past 20–30 k.y. (Dong et al., 2014). The ~1.0 mm/yr estimate on the Lake Range fault is consistent with a vertical slip rate of 0.609–1.096 mm/yr estimated by dePolo (1998).

A lower slip rate on the Lake Range fault occurs south of Anaho Island, an inferred stepover where deformation is transferred to the west along the Pyramid Lake fault. North of Anaho Island, the slip rates on the Lake Range fault increase to ~1.5 mm/yr (Table 1). The fault scarp north of D06L12 (Fig. 6), used to calculate 1.0 mm/yr of vertical slip, shows much greater offsets, though horizons cannot be traced across the fault trace. These limitations indicate that observed rates are a minimum or underestimate rate for the length of the Lake Range fault. Thickening of stratigraphic units into the present-day fault location (Fig. 6) during the late Pleistocene (at the southern terminus of the Lake Range fault) also suggests that this section of the fault is active and may have recently lengthened southward.

Using a vertical slip rate of 1.0 mm/yr and a fault plane dip of 70°, the horizontal extension rate is calculated to be ~0.35 mm/yr (note that the 70° measured dip may not accurately depict the dip at depth, which is beyond CHIRP imaging capability). The ~0.35 mm/yr rate is consistent with the horizontal extension rate measured using GPS block modeling from Hammond et al. (2011) at 0.15 ± 0.26 mm/yr. The slight discrepancy between these rates may be related to a lack of local Pyramid Lake basin GPS stations in the study of Hammond et al. (2011).

Given that the age estimate of the green horizon is extrapolated using sedimentation rates determined from core PLC97-1, there is a possibility that the green reflector may be correlated to the Tsoyawata bed of the Mazama tephra (ca. 7.8 ka; Davis, 1978; Bacon, 1983). In this scenario, the green horizon would then be slightly younger, yielding a higher Holocene slip rate of ~1.2 mm/yr.

Additional Slip Rates

Additional Holocene slip rates were calculated throughout the lake (Table 1; black dots in Fig. 3) using offsets of the 48 ka horizon (blue in Figs. 4–12). The calculations show the progression of slip rates along each of the significant faults in the basin; however, there is some variability along each fault. The combined rates across the lake record substantial vertical motion. These calculations range from 0.07 mm/yr to 0.4 mm/yr (Table 1). The rates are apparent vertical slip rates and possibly underestimate the rate due to the obliquity between the fault trace and the profile. Nevertheless, the data indicate that the Pyramid Lake basin is actively shearing due to the transtension of the northern Walker Lane. The "fanning open" of the northern basin is due to the interaction among the Lake Range normal fault, the dextral shear from the Pyramid Lake fault, and others transtensional faults to the northwest.

Lake Range Fault Seismic Hazards

Many of the active Walker Lane and Basin and Range Province normal faults have been studied through geological trenching and calculated slip rates. The range-bounding normal fault of Smith Valley, Nevada, has a clear ~3.5 m scarp in alluvium from one event, which gives a minimum and maximum slip rate of 0.125 mm/yr and 0.33 mm/yr, respectively (Wesnousky and Caffee, 2011). Through a compilation of various studies, the vertical component of coseismic offset of normal faults along the margins of the basins was found to vary from less than 1 m to greater than 4.5 m (Wesnousky, 2005a), resulting in an average offset of ~2.5 m.

The most active segment of the Lake Range fault (based on the evidence for vertical displacement) in the Holocene lies between line D06L12 and line D03L05, totaling a length of ~15 km. This length is used in calculating the possible length of rupture for an earthquake event. This length gives a range of magnitudes from M6.4 to M6.7 (Wells and Coppersmith, 1994; Wesnousky, 2008). An event rupturing the entire ~41 km length of the Lake Range fault (from the northern tip of the Lake Range to line D06L12) would generate a magnitude M6.9. ± 0.4 event. Despite the uncertainties of this magnitude calculation, an event on this fault would have significant effects on the Reno and Sparks metropolitan areas 64 km to the southwest.

CONCLUSIONS

The dense network of CHIRP profiles collected in the Pyramid Lake basin provide detailed images of fault structure in a highly complex region. For the first time, it is possible to generate a comprehensive fault map beneath the lake itself. The CHIRP imagery records a distinct polarity change in basin architecture from the northwest-striking dextral Pyramid Lake fault in the south onto a combination of the north-striking Lake Range fault and northwest-oriented oblique faults in the northern portion of the basin. Dates from sediment cores within the lake are correlated along CHIRP profiles, providing age estimates for seismic horizons. These ages (combined with >9.5 m of fault offset) give a minimum slip rate of ~1.0 mm/yr on the Lake Range fault. Magnitude estimates suggest potential event sizes between M6.4 and M6.9. The northwest end of the basin is "fanning open" due to a dense network of short, discontinuous dip-slip faults reminiscent of a nascent shear zone. This investigation also helps unravel how strain is transferred between the Great Basin proper to the eastern margin of the northern Walker Lane. Deformation along the Pyramid Lake fault terminates, passing motion onto the Lake Range fault just south of Anaho Island. Toward the north, an additional set of northwest-trending faults displaces the northwestern shoreline.

ACKNOWLEDGMENTS

First and foremost, we wish to thank Donna Noel, John Jackson, and the Pyramid Lake Paiute Tribe for access to Pyramid Lake and its enchanting environment. We wish to thank Larry Benson and Scott Mensing for access to their core data, which helped immensely with the chronologic framework for this project. This manuscript was greatly improved through conversations with Jim Faulds, Steve Wesnousky, and Pat Cashman. An anonymous reviewer and Craig Jones added greatly to this manuscript. We also wish to thank IHS Kingdom for their academic license and access to Kingdom Suite software, and QPS for academic pricing for Fledermaus. This research was funded through a grant from the Bureau of Indian Affairs, and the U.S. Geological Survey National Earthquake Hazards Reduction Program (NEHRP) grant G12AP20110.

REFERENCES CITED

Adams, K.D., Wesnousky, S.G., and Bills, B.G., 1999, Isostatic rebound, active faulting, and potential geomorphic effects in the Lake Lahontan basin, Nevada and California: Geological Society of America Bulletin, v. 111, no. 12, p. 1739–1756, doi:10.1130/0016-7606(1999)111<1739:IRAFAP>2.3.CO;2.

Anderson, L.W., and Hawkins, F.F., 1984, Recurrent Holocene strike-slip faulting, Pyramid Lake fault zone, western Nevada: Geology, v. 12, p. 681–684, doi:10.1130/0091-7613(1984)12<681:RHSFPL>2.0.CO;2.

Argus, D.F., and Gordon, R.G., 1991, Current Sierra Nevada–North America motion from very long baseline interferometry: Implications for the kinematics of the western United States: Geology, v. 19, p. 1085–1088, doi:10.1130/0091-7613(1991)019<1085:CSNNAM>2.3.CO;2.

Atwater, T., 1970, Implications of plate tectonics for the Cenozoic tectonic evolution of western North America: Geological Society of America Bulletin, v. 81, p. 3513–3536, doi:10.1130/0016-7606(1970)81[3513:IOPTFT]2.0.CO;2.

Atwater, T., and Stock, J., 1998, Pacific–North America plate tectonics of the Neogene southwestern United States: An update: International Geology Review, v. 40, p. 375–402, doi:10.1080/00206819809465216.

Bacon, C.R., 1983, Eruptive history of Mount Mazama and Crater Lake caldera, Cascade Range, U.S.A.: Journal of Volcanology and Geothermal Research, v. 18, p. 57–115.

Bell, J.W., and House, P.K., 2005, Pattern and role of late Quaternary faulting along the Pyramid Lake fault zone, northern Walker Lane belt, based on deformation of Lake Lahontan chronostratigraphy: Seismological Society of America Research Letters, v. 76, no. 2, p. 245.

Bell, J.W., House, P.K., and Briggs, R.W., 2003, Preliminary Geologic Map of the West Half of the Nixon Quadrangle, Washoe County, Nevada: Nevada Bureau of Mines and Geology Open-File Report 03–21, scale 1:24,000.

Bell, J.W., House, P.K., and Briggs, R.W., 2004, Preliminary Geologic Map of the East Half of the Pah Rah Mountain Quadrangle, Washoe County, Nevada: Nevada Bureau of Mines and Geology Open-File Report 04–3, scale 1:24,000.

Bennett, R.A., Davis, J.L., and Wernicke, B.P., 1999, Present-day pattern of Cordilleran deformation in the western United States: Geology, v. 27, p. 371–374, doi:10.1130/0091-7613(1999)027<0371:PDPOCD>2.3.CO;2.

Bennett, R.A., Wernicke, B.P., Niemi, N.A., Friedrich, A.M., and Davis, J.L., 2003, Contemporary strain rates in the northern Basin and Range Province from GPS data: Tectonics, v. 22, 1008, doi:10.1029/2001TC001355.

Benson, L.V., and Mifflin, M.D., 1986, Reconnaissance Bathymetry of Basins Occupied by Pleistocene Lake Lahontan, Nevada and California: U.S. Geological Survey Water- Resources Investigations Report 85–4262, 14 p.

Benson, L.V., Kashgarian, M., Rye, R., Lund, S., Paillet, F., Smoot, J., Kester, C., Mensing, S., Meko, D., and Lindstrom, S., 2002, Holocene multidecadal and multicentennial droughts affecting northern California and Nevada: Quaternary Science Reviews, v. 21, p. 659–682, doi:10.1016/S0277-3791(01)00048-8.

Benson, L.V., Smoot, J.P., Lund, S.P., Mensing, S.A., Foit, F.F., Jr., and Rye, R.O., 2013, Insights from a synthesis of old and new climate-proxy data from the Pyramid and Winnemucca Lake basins for the period 48 to 11.5 cal ka: Quaternary International, v. 310, p. 62–82, doi:10.1016/j.quaint.2012.02.040.

Bonham, H.F., and Papke, K.G., 1969, Geology and Mineral Deposits of Washoe and Storey Counties, Nevada: Nevada Bureau of Mines and Geology Bulletin 70, 139 p.

Bosworth, W., 1985, Geometry of propagating continental rifts: Nature, v. 316, p. 625–627, doi:10.1038/316625a0.

Briggs, R.W., and Wesnousky, S.G., 2004, Late Pleistocene fault slip rate, earthquake recurrence, and recency of slip along the Pyramid Lake fault zone, northern Walker Lane, United States: Journal of Geophysical Research, v. 109, p. B08402, doi:10.1029/2003JB002717.

Brothers, D.S., Driscoll, N.W., Kent, G.M., Harding, A.J., Babcock, J.M., and Baskin, R.L., 2009, Tectonic evolution of the Salton Sea inferred from seismic reflection data: Nature Geoscience, v. 2, no. 8, p. 581–584, doi:10.1038/ngeo590.

Cashman, P., and Fontaine, S.A., 2000, Stain partitioning in the northern Walker Lane, western Nevada and northeastern California: Tectonophysics, v. 326, p. 111–130, doi:10.1016/S0040-1951(00)00149-9.

Davis, J.O., 1978, Quaternary Tephrochronolgy of the Lake Lahontan Area, Nevada and California: Nevada Archeological Survey Research Paper 7, 137 p.

dePolo, C.M., 1998, A Reconnaissance Technique for Estimating the Slip Rate of Normal Slip Faults in the Great Basin, and Application to Faults in Nevada, U.S.A. [Ph.D. dissertation]: Reno, Nevada, University of Nevada, 762 p.

Dingler, J., Kent, G., Driscoll, N., Babcock, J., Harding, A., Seitz, G., Karlin, B., and Goldman, C., 2009, A high-resolution seismic CHIRP investigation of active normal faulting across Lake Tahoe Basin, California-Nevada: Geological Society of America Bulletin, v. 121, p. 1089–1107, doi:10.1130/B26244.1.

Dixon, T.H., Miller, M., Farina, F., Wang, H., and Johnson, D., 2000, Present-day motion of the Sierra Nevada block and some tectonic implications for the Basin and Range Province, North American Cordillera: Tectonics, v. 19, p. 1–24, doi:10.1029/1998TC001088.

Dohrenwend, J.C., McKittrick, M.A., and Moring, B.C., 1991, Reconnaissance Photogeologic Map of Young Faults in the Lovelock 1° by 2° Quadrangle, Nevada and California: U.S. Geological Survey Miscellaneous Field Studies Map MF-2178, 1 sheet, scale 1:250,000.

Dokka, R.K., and Travis, C.J., 1990, Role of the Eastern California shear zone in accommodating Pacific–North-American plate motion: Geophysical Research Letters, v. 17, no. 9, p. 1323–1326, doi:10.1029/GL017i009p01323.

Dong, S., Ucarkus, G., Wesnousky, S.G., Maloney, J., Kent, G., Driscoll, N., and Baskin, R., 2014, Strike-slip faulting along the Wassuk Range of the northern Walker Lane: Geosphere, v. 10, no. 1, p. 1–9, doi:10.1130/GES00912.1.

Drakos, P.S., 2007, Tertiary Stratigraphy and Structure of the Southern Lake Range Northwest Nevada: Assessment of Kinematic Links between Strike-Slip and Normal Faults in the Northern Walker Lane [M.S. thesis]: Reno, Nevada, University of Nevada, 179 p.

Driscoll, N.W., Hogg, J.R., Karner, G.D., and Christie-Blick, N., 1995, Extensional tectonics in the Jeanne d'Arc basin, offshore Newfoundland: Implications for the timing of break-up between Grand Banks and Iberia, *in* Scrutton, R.A., Stoker, M.S., Shimmield, G.B., and Tudhope, A.W., eds., The Tectonics, Sedimentation and Palaeoceanography of the North Atlantic Region: Geological Society of London Special Publication 90, p. 1–28.

Eddington, P.K., Smith, R.B., and Renggli, C., 1987, Kinematics of Basin and Range intraplate extension, *in* Howard, M.P., Dewey, J.F., and Hancock, P.L., eds., Continental Extensional Tectonics: Geological Society of London Special Publication 28, p. 371–392.

Ekren, E.B., and Byers, F.M., Jr., 1984, The Gabbs Valley Range—A well-exposed segment of the Walker Lane in west-central Nevada, *in* Lintz, J., Jr., ed., Western Geologic Excursions, Volume 4: Reno, Nevada, Geological Society of America, Annual Meeting Guidebook, p. 203–215.

Ekren, E.B., Byers, F.M., Jr., Hardyman, R.F., Marvin, R.F., and Silberman, M.L., 1980, Stratigraphy, Preliminary Petrology, and Some Structural Features of Tertiary Volcanic Rocks in the Gabbs Valley and Gillis Ranges, Mineral County, Nevada: U.S. Geological Survey Bulletin 1464, 54 p.

Faulds, J.E., and Henry, C.D., 2008, Tectonic influences on the spatial and temporal evolution of the Walker Lane: An incipient transform fault along the evolving Pacific–North American plate boundary, *in* Spencer, J.E., and Titley, S.R., eds., Ores and Orogenesis: Circum-Pacific Tectonics, Geologic Evolution, and Ore Deposits: Arizona Geological Society Digest, v. 22, p. 437–470.

Faulds, J.E., dePolo, C.M., and Henry, C.D., 2003, Geologic Map of the Sutcliffe Quadrangle, Washoe County, Nevada: Nevada Bureau of Mines and Geology Open-File Report 03–17, scale 1:24,000.

Faulds, J.E., Henry, C.D., and Hinz, N.H., 2005a, Kinematics of the northern Walker Lane: An incipient transform fault along the Pacific–North American plate boundary: Geology, v. 33, p. 505–508, doi:10.1130/G21274.1.

Faulds, J.E., Henry, C.D., Hinz, N.H., Drakos, P.S., and Delwiche, B., 2005b, Transect across the northern Walker Lane, northwest Nevada and northeast California: An incipient transform fault along the Pacific–North American plate boundary, *in* Pederson, J.L., and Dehler, C.M., eds., Interior Western United States: Geological Society of America Field Guide 6, p. 129–150.

Flannery, J.W., and Rosendahl, B.R., 1990, The seismic stratigraphy of Lake Malawi, Africa: Implications for interpreting geological processes in lacustrine rifts: Journal of African Earth Sciences, v. 10, no. 3, p. 519–548, doi:10.1016/0899-5362(90)90104-M.

Gilbert, G.K., 1890, Lake Bonneville: U.S. Geological Survey Monograph 1, 438 p.

Hammond, W.C., and Thatcher, W., 2004, Contemporary tectonic deformation of the Basin and Range Province, western United States: 10 years of observation with the global positioning system: Journal of Geophysical Research, v. 109, p. B08403, doi:10.1029/2003JB002746.

Hammond, W.C., Blewitt, G., and Kreemer, C., 2011, Block modeling of crustal deformation of the northern Walker Lane and Basin and Range from GPS velocities: Journal of Geophysical Research, v. 116, B04402, doi:10.1029/2010JB007817.

Hardyman, R.F., 1980, Geologic Map of the Gillis Canyon Quadrangle, Mineral County, Nevada: U.S. Geological Survey Miscellaneous Investigations Map I-1237, scale 1:48,000.

Kent, G.M., Babcock, J.M., Driscoll, N.W., Harding, A.J., Dingler, J.A., Seitz, G.G., Gardner, J.V., Mayer, L.A., Goldman, C.R., Heyvaert, A.C., Richards, R.C., Karlin, R., Morgan, C.W., Gayes, P.T., and Owen, L.A., 2005, 60 k.y. record of extension across the western boundary of the Basin and Range Province: Estimate of slip rates from offset shoreline terraces and a catastrophic slide beneath Lake Tahoe: Geology, v. 33, no. 5, p. 356–368, doi:10.1130/G21230.21231.

Locke, A., Billingsley, P., and Mayo, E., 1940, Sierra Nevada tectonic patterns: Geological Society of America Bulletin, v. 51, p. 513–539, doi:10.1130/GSAB-51-513.

McQuarrie, N., and Wernicke, B.P., 2005, An animated tectonic reconstruction of southwestern North America since 36 Ma: Geosphere, v. 1, no. 3, p. 147–172, doi:10:1130/GES00016.1.

Mensing, S.A., Benson, L.V., Kashgarian, M., and Lund, S., 2004, A Holocene pollen record of persistent droughts from Pyramid Lake, Nevada, USA: Quaternary Research, v. 62, p. 29–38, doi:10.1016/j.yqres.2004.04.002.

Nagorsen-Rinke, S., Lee, J., and Calvert, A., 2013, Pliocene sinistral slip across the Adobe Hills, eastern California–western Nevada: Kinematics of fault slip transfer across the Mina deflection: Geosphere, v. 9, no. 1, p. 37–53, doi:10.1130/GES00825.1.

Oldow, J.S., 1992, Late Cenozoic displacement partitioning in the northwestern Great Basin, *in* Craig, S.D., ed., Structure, Tectonics, and Mineralization of the Walker Lane; Walker Lane Symposium, Proceedings Volume: Reno, Nevada, Geological Society of Nevada, p. 17–52.

Oldow, J.S., 2003, Active transtensional boundary zone between the western Great Basin and Sierra Nevada block, western U.S. Cordillera: Geology, v. 31, p. 1033–1036, doi:10.1130/G19838.1.

Ramelli, A.R., Bell, J.W., dePolo, C.M., and Yount, J.C., 1999, Large-magnitude, late Holocene earthquakes on the Genoa fault, west-central Nevada and eastern California: Bulletin of the Seismological Society of America, v. 89, p. 1458–1472.

Rosendahl, B.R., Kilembe, E., and Kaczmarick, K., 1992, Comparison of the Tanganyika, Malawi, Rukwa and Turkana rift zones from analysis of seismic reflection data: Tectonophysics, v. 213, p. 235–256, doi:10.1016/0040-1951(92)90261-4.

Sawyer, T.L., and Adams, K.D., compilers, 1999, Fault number 1607, Eastern Pyramid Lake fault, *in* Quaternary Fault and Fold Database of the United States: U.S. Geological Survey, http://earthquakes.usgs.gov/hazards/qfaults (accessed March 2015).

Schwartz, D.P., and Coppersmith, K.J., 1984, Fault behavior and characteristic earthquakes: Examples from the Wasatch and San Andreas fault zones: Journal of Geophysical Research–Solid Earth, v. 89, p. 5681–5698, doi:10.1029/JB089iB07p05681.

Stewart, J.H., 1988, Tectonics of the Walker Lane belt, western Great Basin: Mesozoic and Cenozoic deformation in a zone of shear, *in* Ernst, W.G., ed., Metamorphism and Crustal Evolution of the Western United States: Englewood Cliffs, New Jersey, Prentice Hall, p. 681–713.

Svarc, J.L., Savage, J.C., Prescott, W.H., and Ramelli, A.R., 2002, Strain accumulation and rotation in western Nevada, 1993–2000: Journal of Geophysical Research, v. 107, no. B5, doi:10.1029/2001JB000579.

Thatcher, W., 2003, GPS constraints on the kinematics of continental deformation: International Geology Review, v. 45, p. 191–212, doi:10.2747/0020-6814.45.3.191.

Thatcher, W., Foulger, G.R., Julian, B.R., Svarc, J.L., Quilty, E., and Bawden, G.W., 1999, Present-day deformation across the Basin and Range Province, western United States: Science, v. 283, p. 1714–1718, doi:10.1126/science.283.5408.1714.

Trexler, J.H., Jr., Park, H.M., and Cashman, P.H., 2009, Late Neogene basin history at Honey Lake, northeastern California: Implications for regional tectonics at 3 to 4 Ma, *in* Oldow, J.S., and Cashman, P.H., eds., Late Cenozoic Structure and Evolution of the Great Basin–Sierra Nevada Transition: Geological Society of America Special Paper 447, p. 83–100, doi:10.1130/2009.2447(06).

Turner, R., Koehler, R.D., Briggs, R.W., and Wesnousky, S.G., 2008, Paleoseismic and slip-rate observations along the Honey Lake fault zone, northeastern California, USA: Bulletin of the Seismological Society of America, v. 98, p. 1730–1736, doi:10.1785/0120070090.

Unruh, J.R., Humphrey, J., and Barron, A., 2003, Transtensional model for the Sierra Nevada frontal fault system, eastern California: Geology, v. 31, no. 4, p. 327–330, doi:10.1130/0091-7613(2003)031<0327:TMFTSN>2.0.CO;2.

Wells, D.L., and Coppersmith, K.J., 1994, New empirical relationships among magnitude, rupture length, rupture width, rupture area, and surface displacement: Bulletin of the Seismological Society of America, v. 84, p. 974–1002.

Wesnousky, S.G., 2005a, Active faulting in the Walker Lane: Tectonics, v. 24, TC3009, doi:10.1029/2004TC001645.

Wesnousky, S.G., 2005b, The San Andreas and Walker Lane fault systems, western North America: Transpression, transtension, cumulative slip and the structural evolution of a major transform plate boundary: Journal of Structural Geology, v. 27, p. 1505–1512, doi:10.1016/j.jsg.2005.01.015.

Wesnousky, S.G., 2008, Displacement and geometrical characteristics of earthquake surface ruptures: Issues and implications for seismic hazard analysis and the process of earthquake rupture: Bulletin of the Seismological Society of America, v. 98, no. 4, p. 1609–1632, doi:10.1785/0120070111.

Wesnousky, S.G., and Caffee, M., 2011, Range-bounding normal fault of Smith Valley, Nevada: Limits on age of last surface-rupture earthquake and late Pleistocene rate of displacement: Bulletin of the Seismological Society of America, v. 101, no. 3, p. 1431–1437, doi:10.1785/0120100238.

Wesnousky, S.G., Baron, A.D., Briggs, R.W., Caskey, J.S., Kumar, S.J., and Owen, L., 2005, Paleoseismic transect across the northern Great Basin: Journal of Geophysical Research, v. 110, p. B05408, doi:10.1029/2004JB003283.